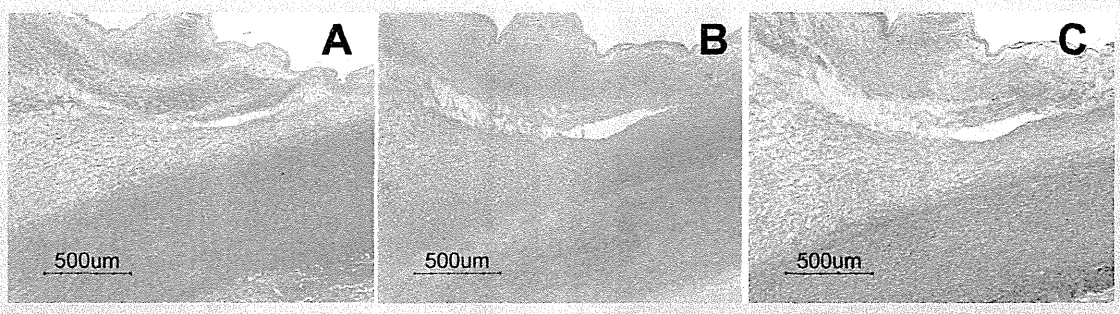

FIG. 3. Histology of the resected aorta of Patient 2. A: Nodular hypertrophy of the inner media by hyperplasia of smooth muscle cells. Hematoxylin–eosin stain. B: Diffuse mucoid accumulation, and separation and irregular layers of the smooth muscle cells in the same inner media. Alcian blue stain. C: Fragmentation, reduction, and separation of the elastica and hyperplasia of the collagen fiber in the above media. Elastica-van Gieson stain.

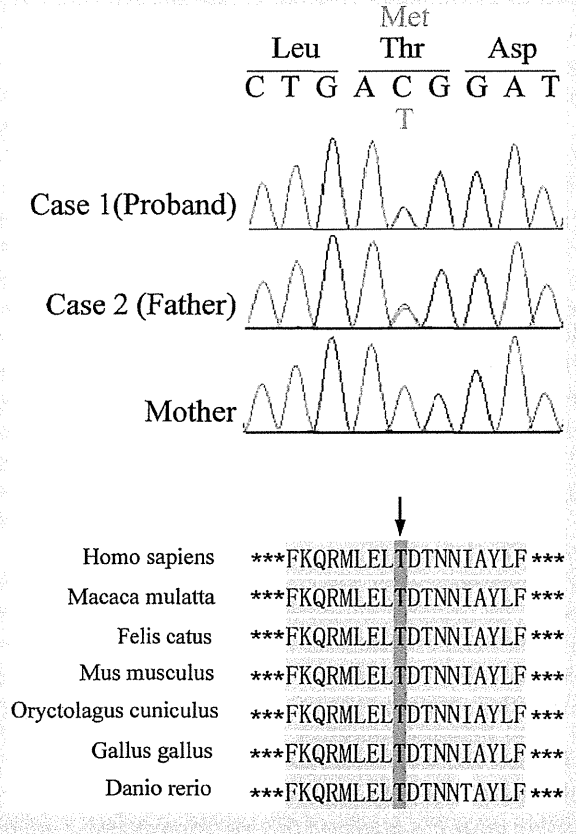

FIG. 4. A missense mutation, c.3605C → T (p.T1202M) at exon 29 of *ABCC9* in Patient 1 (upper) and 2 (lower). p.T1202 is evolutionally conserved from fish to mammals (CLUSTALW ver. 2.1: http://clustalw.ddbj.nig.ac.jp/top-j.html).

In addition, no pathogenic aberrations in the genes causing thoracic aneurysm, including *ACTA2*, *COL3A1*, *FBN1*, *GLUT10*, *MYH11*, *PLOD1*, *TGFBR1*, *TGFBR2*, *SMAD3*, and *TGFB2* were not found in the affected father by whole exome sequencing.

DISCUSSION

The facial dysmorphism and congenital hypertrichosis in the affected boy and father warranted a diagnosis of Cantu syndrome in the present family. However, macrosomia was observed only in the father, while cardiomegaly only in the son. The prenatal cardiac problem (pericardial effusion) in the son may have accounted for the absence of macrosomia. The unique manifestations in this family were thoracic aortic aneurysm in the father and craniosynostosis in the son. Primary craniosynostosis was considered based on absence of microcephaly and a couple of imaging findings such as a copper beaten appearance of the calvaria and normal brain structures. The pathogenic *ABCC9* abnormality (c.3605C > T, p.T1202M) in this family was a novel missense mutation. The mutation was located in the TMD2 (transmembrane domain 2) of ABCC9, like previously reported mutations in Cantu syndrome, most of which were found either in TMD1 or TMD2 [Harakalova et al., 2012; van Bon et al., 2012].

The pathogenesis of *ABCC9* mutations remains incompletely understood. Yet, recent investigations have provided some clues to understanding the consequence of *ABCC9* mutation. Alternative RNA splicing of the terminal exon (exon 38) of *ABCC9* yields two SUR2 isoforms (SUR2A and SUR2B), which differ only in their C-terminal 42 amino acids. SUR2A is predominantly expressed in cardiac and skeletal muscle cells, while SUR2B is expressed in vascular smooth muscle, hair follicles, and some neurons. Loss-of-function mutations in the terminal exon that impair only SUR2A result in dilated cardiomyopathy [Bienengraeber et al., 2004] and familial atrial fibrillation [Olson et al., 2007]. Conversely, all 27 mutations previously identified in Cantu syndrome are located upstream of the terminal exon and; therefore, interfere with both

SUR2A and SUR2B. The different expression patterns between *ABCC9* isoforms and different mutation pattern between Cantu syndrome and other genetic heart diseases explain different clinical manifestations of these disorders. The expression pattern accounts for the aortic aneurysm seen in Patient 2 as well as cardiomegaly and hypertrichosis in Cantu syndrome.

Moreover, it is postulated that *ABCC9* mutations in Cantu syndrome may produce gain-of-function proteins [Harakalova et al., 2012]. Consistent with this presumption, cardiomegaly in Cantu syndrome is associated with ventricular hypertrophy, which contrasts with the dilated cardiomyopathy observed in ABCC9 loss-of-function. K(ATP) channels (ATP-sensitive potassium channels), including ABCC9, are characterized by inhibition of channel opening at increased ATP concentration on the cytoplasmic cell surface. At the basal condition, ABCC9 is closed [Koster et al., 2001; Flagg et al., 2004]. At a low metabolic state, it is open, resulting in K^+ efflux, membrane hyperpolarization, reduced Ca^{2+} influx, shorter action potentials, higher cardiac output and vasodilation. These biological consequences ensure perfusion to the brain and heart following an ischemic challenge [Wind et al., 1997]. Thus, the major biological role of ABCC9 may be protection from ischemic stress in the heart, protection against fiber damage in skeletal muscle, and control of vasomotor tone in smooth muscle when energy supplies are low.

A report focusing on cardiovascular effects of ABCC9 overexpression stated that even at the low metabolic state (in the absence of elevated ATP/ADP ratio), K(ATP) channel openers, such as cromakalin, were still able to produce further acceleration of opening of ABCC9, resulting in vasodilation [D'Hahan et al., 1999]. Overexpression of SUR2A in transgenic mice generated a cardiac phenotype resistant to hypoxia/ischemia/reperfusion injury [Du et al., 2006]. Treatment with K(ATP) channel openers in rat has been shown to stabilize resting membrane potential and reduce the frequency of arrhythmias in some studies [Du et al., 2006], but has proven proarrhythmic in others [Zhou et al., 2005]. Despite the basic protective effect of ABCC9 on the heart, its persistent overactivity may cause ventricular hypertrophy and eventual cardiac failure. The vasodilative effect of ABCC9 may be related to the aortic aneurysm in Patient 2.

Cardiac problems are a potentially lethal association in Cantu syndrome. Based on a review of the literature (n = 58, mean age: 8 9/12 years, range: 3 months to 50 years), the cardiac phenotype in Cantu syndrome is summarized in Table I. A small subset of patients had normal cardiac function; however, most patients presented with ventricular hypertrophy with diastolic dysfunction, which ultimately can evolve into systolic dysfunction associated with pulmonary hypertension, mitral regurgitation/insufficiency, and tricuspid regurgitation/insufficiency (if present). Onset of heart problems is quite variable among affected individuals, ranging from the prenatal period to young adulthood. Interestingly, cardiac function may wax and wane regardless of presence or absence of medical intervention. Some patients showed aortic regurgitation,

TABLE I. Cardiac Manifestations in Cantu Syndrome

	Patient 1	Patient 2	Previously reported patients (n = 58)
Age	4 years 0 months	31 years	8.9 years (3.5 months to 50 years)[a]
Cardiomegaly	+	−	43/54[b]
Pericardial effusion	+	−	9/51[b]
Thoracic aortic aneurysm	−	+	0/57[b]
Congenital heart defects	−	−	25/52[b]
PDA	−	−	16/47[b]
Cardiac hypertrophy			27/44[b]
Cardiomyopathy	−	−	7/44[b]
Cardiac hypertrophy	−	−	20/44[b]
Left ventricular hypertrophy	−	−	12/44[b]
Biventricular hypertrophy	−	−	4/44[b]
Right ventricular hypertrophy	−	−	2/44[b]
Dilated left ventricle	+	−	2/44[b]
Hemodynamic abnormalities		−	21/39[b]
Pulmonary hypertension	+	−	7
Tricuspid regurgitation/tricuspid incompetence	−	−	7
Mitral regurgitation/mitral incompetence	−	−	5
Aortic regurgitation	−	−	2
Dyspnea on excise	+	−	3
Orthopnea	−	−	1
Cardiac failure	+	−	6

[a]Average (range of age).
[b]Number of patients having the condition/number of patients examined for the condition (these data have previously been reported in Hum Genet 60:36–41, 1982; Am J Med Genet 66:33–38, 1996; Am J Med Genet 69:138–151, 1997; Clin Dysmorphol 7:79–85, 1998; Am J Med Genet 85:395–402, 1999; Am J Med Genet 92:191–194, 2000; Am J Med Genet 94:421–427, 2000; Am J Med Genet 111:205–209, 2002; Am J Med Genet A 140:1673–1680, 2006; Pediatr Pulmonol 45:727–729, 2010; Clin Dysmorphol 20:32–37, 2011; Am J Med Genet A 155A:508–18, 2011; Am J Med Genet A 155A:1184–1188, 2011; Am J Hum Genet 90:1094–1101, 2012; Nat Genet 44:793–796, 2012; Am J Med Genet A 161A:295–300, 2013).

which may have implied aortic dilatation. In the present family, the cardiac phenotypes were different between the two patients. The affected boy had prenatal pericardial effusion and postnatal cardiomegaly, while the affected father did not have overt cardiac problems. Thus, the cardiac phenotype in Cantu syndrome is not determined by the genotype alone.

Macrosomia and mild osteochondrodysplasia are other hallmarks of Cantu syndrome. The skeletal manifestation varies among patients. The present patients did not show any overt skeletal alterations. The biological roles of ABCC9 in somatic and skeletal growth remain unsolved. These issues may be elucidated in the context of the role of ABCC9 as a sulfonylurea receptor. The SUR subunits of K(ATP) channel have been recognized as an ATPase. As the SUR proteins show a conformational modification following changes in ATP content, the SUR subunits are presumed to work as a mechanochemical device, and may play a pivotal role in somatic and bone development [Karpowich et al., 2001; Zingman et al., 2002; Jons et al., 2006]. In fact, it is known that ABCC9 can regulate paracellular permeability in gastrointestinal, renal and liver tissues [Jons et al., 2006]. The role of ABCC9 as a mechnochemical senser may possibly be important in development of the cranial sutures and calvarial intramembranous ossification.

In conclusion, we found a family in which both son and father are affected with Cantu syndrome caused by an *ABCC9* mutation. Craniosynostosis in the boy and development of aortic aneurysm in the father were previously undescribed associations with Cantu syndrome.

ACKNOWLEDGMENTS

We thank the family for participating in this work. We also thank Ms. S. Sugimoto, Ms. N. Watanabe, Ms. K. Takabe, and Mr. T. Miyama for their technical assistance. This work was supported by research grants from the Ministry of Health, Labour and Welfare of Japan (N. Miyake, N. Matsumoto), the Japan Science and Technology Agency (N. Matsumoto), the Strategic Research Program for Brain Sciences (N. Matsumoto), a Grant-in-Aid for Scientific Research on Innovative Areas-(Transcription cycle)-from the Ministry of Education, Culture, Sports, Science and Technology of Japan (N. Miyake, N. Matsumoto), a Grant-in-Aid for Scientific Research from the Japan Society for the Promotion of Science (H.S., N. Miyake, N. Matsumoto), the Takeda Science Foundation (N. Miyake, N. Matsumoto), the Yokohama Foundation for the Advancement of Medical Science (N. Miyake), and the Hayashi Memorial Foundation for Female Natural Scientists (N. Miyake).

REFERENCES

Bienengraeber M, Olson TM, Selivanov VA, Kathmann EC, O'Cochlain F, Gao F, Karger AB, Ballew JD, Hodgson DM, Zingman LV, Pang YP, Alekseev AE, Terzic A. 2004. ABCC9 mutations identified in human dilated cardiomyopathy disrupt catalytic KATP channel gating. Nat Genet 36:382–387.

Cantu JM, Garcia-Cruz D, Sanchez-Corona J, Hernandez A, Nazara Z. 1982. A distinct osteochondrodysplasia with hypertrichosis—Individualization of a probable autosomal recessive entity. Hum Genet 60:36–41.

DePristo MA, Banks E, Poplin R, Garimella KV, Maguire JR, Hartl C, Philippakis AA, del Angel G, Rivas MA, Hanna M, McKenna A, Fennell TJ, Kernytsky AM, Sivachenko AY, Cibulskis K, Gabriel SB, Altshuler D, Daly MJ. 2011. A framework for variation discovery and genotyping using next-generation DNA sequencing data. Nat Genet 43:491–498.

D'Hahan N, Jacquet H, Moreau C, Catty P, Vivaudou M. 1999. A transmembrane domain of the sulfonylurea receptor mediates activation of ATP-sensitive K(+) channels by K(+) channel openers. Mol Pharmacol 56:308–315.

Du Q, Jovanovic S, Clelland A, Sukhodub A, Budas G, Phelan K, Murray-Tait V, Malone L, Jovanovic A. 2006. Overexpression of SUR2A generates a cardiac phenotype resistant to ischemia. FASEB J 20:1131–1141.

Flagg TP, Charpentier F, Manning-Fox J, Remedi MS, Enkvetchakul D, Lopatin A, Koster J, Nichols C. 2004. Remodeling of excitation-contraction coupling in transgenic mice expressing ATP-insensitive sarcolemmal KATP channels. Am J Physiol Heart Circ Physiol 286:H1361–H1369.

Flagg TP, Enkvetchakul D, Koster JC, Nichols CG. 2010. Muscle KATP channels: Recent insights to energy sensing and myoprotection. Physiol Rev 90:799–829.

Harakalova M, van Harssel JJ, Terhal PA, van Lieshout S, Duran K, Renkens I, Amor DJ, Wilson LC, Kirk EP, Turner CL, Shears D, Garcia-Minaur S, Lees MM, Ross A, Venselaar H, Vriend G, Takanari H, Rook MB, van der Heyden MA, Asselbergs FW, Breur HM, Swinkels ME, Scurr IJ, Smithson SF, Knoers NV, van der Smagt JJ, Nijman IJ, Kloosterman WP, van Haelst MM, van Haaften G, Cuppen E. 2012. Dominant missense mutations in ABCC9 cause Cantu syndrome. Nat Genet 44:793–796.

Jons T, Wittschieber D, Beyer A, Meier C, Brune A, Thomzig A, Ahnert-Hilger G, Veh RW. 2006. K+-ATP-channel-related protein complexes: Potential transducers in the regulation of epithelial tight junction permeability. J Cell Sci 119:3087–3097.

Karpowich N, Martsinkevich O, Millen L, Yuan YR, Dai PL, MacVey K, Thomas PJ, Hunt JF. 2001. Crystal structures of the MJ1267 ATP binding cassette reveal an induced-fit effect at the ATPase active site of an ABC transporter. Structure 9:571–586.

Koster JC, Knopp A, Flagg TP, Markova KP, Sha Q, Enkvetchakul D, Betsuyaku T, Yamada KA, Nichols CG. 2001. Tolerance for ATP-insensitive K(ATP) channels in transgenic mice. Circ Res 89:1022–1029.

Olson TM, Alekseev AE, Moreau C, Liu XK, Zingman LV, Miki T, Seino S, Asirvatham SJ, Jahangir A, Terzic A. 2007. KATP channel mutation confers risk for vein of Marshall adrenergic atrial fibrillation. Nat Clin Pract Cardiovasc Med 4:110–116.

van Bon BW, Gilissen C, Grange DK, Hennekam RC, Kayserili H, Engels H, Reutter H, Ostergaard JR, Morava E, Tsiakas K, Isidor B, Le Merrer M, Eser M, Wieskamp N, de Vries P, Steehouwer M, Veltman JA, Robertson SP, Brunner HG, de Vries BB, Hoischen A. 2012. Cantu syndrome is caused by mutations in ABCC9. Am J Hum Genet 90:1094–1101.

Wang K, Li M, Hakonarson H. 2010. ANNOVAR: Functional annotation of genetic variants from high-throughput sequencing data. Nucleic Acids Res 38:e164.

Wind T, Prehn JH, Peruche B, Krieglstein J. 1997. Activation of ATP-sensitive potassium channels decreases neuronal injury caused by chemical hypoxia. Brain Res 751:295–299.

Zhou M, Tanaka O, Sekiguchi M, He HJ, Yasuoka Y, Itoh H, Kawahara K, Abe H. 2005. ATP-sensitive K+-channel subunits on the mitochondria and endoplasmic reticulum of rat cardiomyocytes. J Histochem Cytochem 53:1491–1500.

Zingman LV, Hodgson DM, Bienengraeber M, Karger AB, Kathmann EC, Alekseev AE, Terzic A. 2002. Tandem function of nucleotide binding domains confers competence to sulfonylurea receptor in gating ATP-sensitive K+ channels. J Biol Chem 277:14206–14210.

Neurogenetics
DOI 10.1007/s10048-013-0384-7

ORIGINAL ARTICLE

PIGN mutations cause congenital anomalies, developmental delay, hypotonia, epilepsy, and progressive cerebellar atrophy

Chihiro Ohba · Nobuhiko Okamoto · Yoshiko Murakami · Yasuhiro Suzuki · Yoshinori Tsurusaki · Mitsuko Nakashima · Noriko Miyake · Fumiaki Tanaka · Taroh Kinoshita · Naomichi Matsumoto · Hirotomo Saitsu

Received: 2 November 2013 / Accepted: 10 November 2013

Abstract Defects of the human glycosylphosphatidylinositol (GPI) anchor biosynthetic pathway show a broad range of clinical phenotypes. A homozygous mutation in *PIGN*, a member of genes involved in the GPI anchor-synthesis pathway, was previously reported to cause dysmorphic features, multiple congenital anomalies, severe neurological impairment, and seizure in a consanguineous family. Here, we report two affected siblings with compound heterozygous *PIGN* mutations [c.808T >C (p.Ser270Pro) and c.963G >A] showing congenital anomalies, developmental delay, hypotonia, epilepsy, and progressive cerebellar atrophy. The c.808C >T mutation altered an evolutionarily conserved amino acid residue (Ser270), while reverse transcription-PCR and sequencing demonstrated that c.963G >A led to aberrant splicing, in which two mutant transcripts with premature stop codons (p.Ala322Valfs*24 and p.Glu308Glyfs*2) were generated. Expression of GPI-anchored proteins such as CD16 and CD24 on granulocytes from affected siblings was

Chihiro Ohba, Nobuhiko Okamoto, and Yoshiko Murakami contributed equally

Electronic supplementary material The online version of this article (doi:10.1007/s10048-013-0384-7) contains supplementary material, which is available to authorized users.

C. Ohba · Y. Tsurusaki · M. Nakashima · N. Miyake · N. Matsumoto · H. Saitsu (✉)
Department of Human Genetics, Graduate School of Medicine, Yokohama City University, 3-9 Fukuura, Kanazawa-ku, Yokohama 236-0004, Japan
e-mail: hsaitsu@yokohama-cu.ac.jp

C. Ohba
e-mail: t116017g@yokohama-cu.ac.jp

Y. Tsurusaki
e-mail: tsurusak@yokohama-cu.ac.jp

M. Nakashima
e-mail: mnakashi@yokohama-cu.ac.jp

N. Miyake
e-mail: nmiyake@yokohama-cu.ac.jp

N. Matsumoto
e-mail: naomat@yokohama-cu.ac.jp

C. Ohba · F. Tanaka
Department of Clinical Neurology and Stroke Medicine, Yokohama City University, Yokohama 236-0004, Japan

F. Tanaka
e-mail: ftanaka@yokohama-cu.ac.jp

N. Okamoto
Department of Medical Genetics, Osaka Medical Center and Research Institute for Maternal and Child Health, Izumi 594-1101, Japan
e-mail: okamoto@osaka.email.ne.jp

Y. Murakami · T. Kinoshita
Department of Immunoregulation, Research Institute for Microbial Diseases, Osaka University, Osaka 565-0871, Japan

Y. Murakami
e-mail: yoshiko@biken.osaka-u.ac.jp

T. Kinoshita
e-mail: tkinoshi@biken.osaka-u.ac.jp

Y. Murakami · T. Kinoshita
World Premier International Immunology Frontier Research Center, Osaka University, Osaka 565-0871, Japan

Y. Suzuki
Department of Pediatric Neurology, Osaka Medical Center and Research Institute for Maternal and Child Health, Osaka, Japan
e-mail: yasuzuki@mch.pref.osaka.jp

Published online: 20 November 2013

significantly decreased, and expression of the GPI-anchored protein CD59 in *PIGN*-knockout human embryonic kidney 293 cells was partially or hardly restored by transient expression of p.Ser270Pro and p.Glu308Glyfs*2 mutants, respectively, suggesting severe and complete loss of PIGN activity. Our findings confirm that developmental delay, hypotonia, and epilepsy combined with congenital anomalies are common phenotypes of *PIGN* mutations and add progressive cerebellar atrophy to this clinical spectrum.

Keywords Cerebellar atrophy · Compound heterozygous mutation · Glycosylphosphatidylinositol anchor · *PIGN*

Introduction

Defects of the biosynthetic pathway of the glycosylphosphatidylinositol (GPI) anchor cause broad clinical phenotypes [1]. The products of more than 20 genes in the phosphatidylinositol glycan (PIG) family are involved in GPI biosynthesis, whereas post-GPI-attachment to proteins (PGAP) gene products play a role in the structural remodeling of GPI glycan and lipid portions [2]. Mutations in eight genes involved in GPI biosynthesis and remodeling (*PIGA*, *PIGM*, *PIGN*, *PIGV*, *PIGL*, *PIGO*, *PIGT*, and *PGAP2*) have been identified in individuals with neurological abnormalities [1, 3–5], of which *PIGN* controls the addition of phosphoethanolamine to the first mannose in GPI [6]. To date, only one homozygous *PIGN* mutation has been reported to cause dysmorphic features, multiple congenital anomalies, severe neurological impairment, and seizures in a consanguineous family [7]. Here, we report a family with two affected siblings, possessing compound heterozygous *PIGN* mutations. Detailed clinical information and molecular and functional analyses are presented.

Patients and methods

Patients

We analyzed two affected siblings and their parents. Experimental protocols were approved by the Institutional Review Board of Yokohama City University School of Medicine. Clinical information and peripheral blood samples were acquired from the family members after obtaining written informed consent. Patient clinical features are summarized in Table 1. They showed dysmorphic facial features, developmental delay, intellectual disability, hypotonia, vertical nystagmus, and epilepsy.

Patient 1

This 9-year-old girl was born to nonconsanguineous healthy parents as a second child after 39 weeks of gestation (Fig. 1a). Her birth weight was 3,390 g [+1.40 standard deviation (SD)], body length of 49 cm (−0.03 SD), and head circumference of 35 cm (+1.35 SD). At 1 month of age, she showed vertical nystagmus without eye pursuit. She was hypotonic, and severe developmental delay was evident from early infancy. She was unable to control her head or utter words at 9 years of age. Abdominal echogram revealed bilateral vesicoureteral reflux as a cause of repeated urinary tract infections. Complex partial seizures developed at 8 months of age and were controlled by antiepileptic drugs. Tube feeding by gastrostomy was necessary for poor appetite at the age of 2 years.

Several dysmorphic features (prominent occiput, bitemporal narrowing, epicanthal folds, open mouth, tented upper lip, high arched palate, micrognathia, and deep plantar groove) were noted (Fig. 1b), but hypoplasia was absent from fingers and fingernails. Initial brain magnetic resonance imaging (MRI) at 6 months of age was normal, but cerebellar atrophy was observed at 2 and 6 years of age (Fig. 1c–f).

At present, her height is 122 cm (+1.1 SD), weight of 18.4 kg (−1.2 SD), and head circumference of 51.4 cm (−0.3 SD). Generalized muscle weakness and nystagmus were neurologically recognized. Laboratory examination showed a normal profile, including blood cell count and blood smear, renal and liver function, total bilirubin, uric acid, albumin, serum electrolytes, lactate, pyruvate, ammonia, amino acids, blood gasses, thyroid function, and cerebrospinal fluid study. Her serum alkaline phosphatase (ALP) activity has been normal for her age since infancy. Metabolic disorder screening including organic acid analysis, lysosomal enzymes, and mass spectrometry of transferrin was normal. G-banded analysis showed a normal karyotype (46, XX).

Patient 2

This 2-year-old boy was born after 37 weeks of gestation as a younger brother to patient 1 (Fig. 1a). His birth weight was 3,252 g (+1.3 SD), body length of 50 cm (+1.2 SD), and head circumference of 35 cm (+1.6 SD). He also showed vertical nystagmus at 1 month of age. Complex partial seizures developed at 5 months of age. He was hypotonic, and his developmental milestones were severely delayed with no head control at 1 year and 10 months of age. At present, his height is 92.3 cm (+2.5 SD), weight of 10.9 kg (−0.6 SD), and head circumference of 48.8 cm (+0.4 SD). He showed similar dysmorphic features to patient 1. Brain MRI at 2 months of age revealed no significant abnormalities.

Table 1 Clinical features of patients with *PIGN* mutations

Patient	1	2	Reported by Maydan et al. [7]							
			V-1	V-2	V-4	V-5	V-8	V-9	V-10	Total
Age (years)	9	2	N.D.	Diseased at 14	Diseased at 1	Diseased at 5	Diseased at 3	Diseased at 17	Diseased at 39	
Sex	Female	Male	Male	Male	Male	Female	Female	Female	Male	
Size at birth (percentile)										
Weight (g)	3,390 (90–97)	3,252 (90–97)	3,566 (95)	4,065 (97)	3,850 (95)	3,410 (40)	4,250 (99)	4,300 (98)	4,800 (>99)	
Head circumference (cm)	35 (90)	35 (90–97)	37 (>97)	37 (97)	35.5 (75)	34.5 (10)	N.D.	N.D.	N.D.	
Abnormalities										
Facial features	+	+	+	+	+	+	+	+	+	9/9
Fingers/foot	+	+	+	+	+	-	–	+	+	6/9
Heart	–	–	+	+	+	+	–	+	–	5/9
Urinary tract	+	–	+	+	+	–	–	–	–	4/9
Gastrointestinal tract	GER	–	GER	GER	Anal stenosis	Imperforate anus, ano-vestibular fistula, GER	–	Feeding and swallowing difficulties	Feeding and swallowing difficulties	7/9
Neurological features										
Developmental delay	+	+	+	+	+	+	+	+	+	9/9
Hypotonia	+	+	+	+	+	+	+	+	+	9/9
Nystagmus	+	+	+	+	–	+	–	+	+	7/9
Tremor	+	+	+	+	+	+	+	–	–	7/9
Seizure	+	+	+	–	+	+	+	+	+	8/9
Brain CT	Normal	Normal	Normal	N.D.	Normal	Multiple small subdural hematomas	N.D.	N.D.	N.D.	1/5
Brain MRI				N.D.	N.D.		N.D.	N.D.	N.D.	
Delayed myelination	+	–	–			+				2/4
Thin corpus callosum	–	–	–			+				1/4
Cerebellar atrophy	+	–	Minimal loss of vermis parenchyma			–				1/4
Enlargement of the ventricle	+	–	–			+ (Mild)				2/4

GER Gastroesophageal reflux, *N.D.* not determined

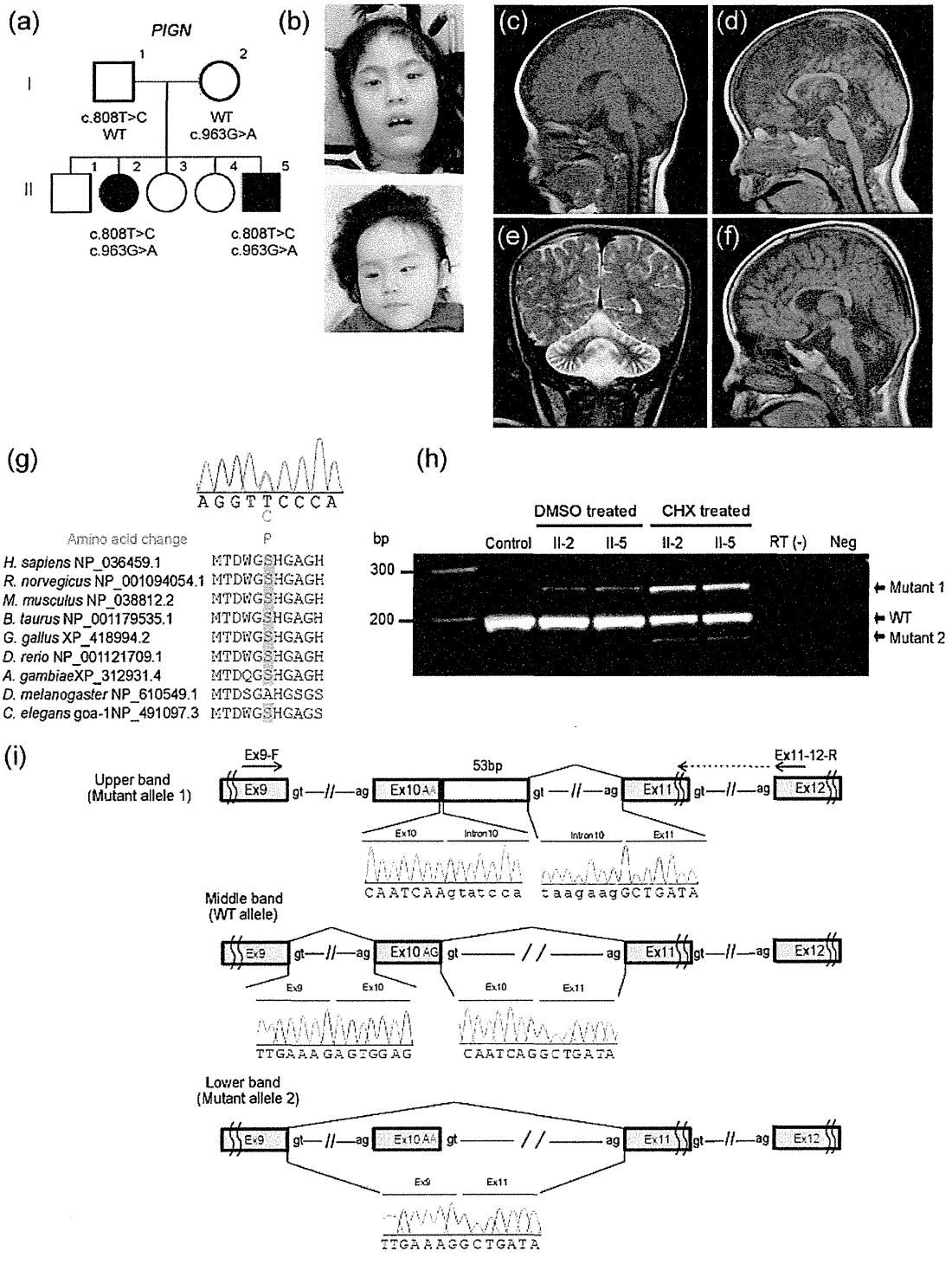

Whole exome sequencing (WES)

Genomic DNA was isolated from peripheral blood leukocytes, captured using the SureSelect Human All Exon v4 Kit (51 Mb; Agilent Technologies, Santa Clara, CA), and sequenced on an Illumina HiSeq2000 (Illumina, San Diego, CA) with 101 bp paired-end reads. Data processing, variant calling, and variant annotation were performed as previously described [8].

Fig. 1 **a** Familial pedigree and mutations. **b** Photographs of the faces of patient 1 (*upper*) and patient 2 (*lower*). Frontal narrow temporal, frontal bossing, hypertelorism, epicanthal folds, down-slanting palpebral fissures, high nasal bridge, bilateral low set ears, thin philtrum, downturned mouth, and microretrognathia are noted in both patients. **c**, **d**, **f** T1-weighted midline sagittal images and **e** T2-weighted coronal images of patient 1 (**c** at 6 months, **d** and **e** at 2 years, and **i** at 6 years). Progressive vermis atrophy (**c**, **d**, **f**) and hemispheres atrophy (**e**) were observed. **g** Sequence chromatography showing heterozyogous c.808C >T mutation, which alters an evolutionarily conserved amino acid. Homologous sequences were aligned using CLUSTALW. **h** RT-PCR analysis using cDNA of LCLs derived from two patients (II-2 and II-5) and a control. **i** Schematic representation of wild-type (WT) and mutant transcripts and primers used for the analysis. Primer of ex11-12-R spans exons 11 and 12. A single band (200 bp), corresponding to the WT allele, was amplified using control cDNA. Upper and lower bands were detected from patient cDNA. The upper band (253 bp) has a 53-bp insertion of intron 10 sequences, leading to a frameshift mutation. The lower band has a 41-bp deletion of the entire exon 10, also leading to a frameshift mutation

Reverse transcriptase-PCR

Lymphoblastoid cell lines (LCLs) were established from the two patients. RT-PCR using total RNA extracted from LCLs was performed as previously described [9].

Briefly, total RNA was extracted using the RNeasy Plus Mini kit (Qiagen, Tokyo, Japan) from LCLs with or without incubation in 30 μM cycloheximide (CHX; Sigma, Tokyo, Japan) for 4 h. Four micrograms of total RNA was subjected to reverse transcription, and 2 μl cDNA was used for PCR. Primer sequences were ex9-F (5′-TCCTTTAGTCACTTGG GGAGCTGGA-3′) and ex11-12-R (5′-AATCCACAGGAA GGATTCCCACTGA-3′) (Supplementary Table 1). PCR products were electrophoresed on a 10 % polyacrylamide gel and sequenced. PCR bands were purified by the E.Z.N.A. poly-Gel DNA Extraction kit (Omega Bio-Tek, Norcross, GA).

Fluorescence-activated cell sorting (FACS) analysis

Surface expression of GPI-anchored proteins (GPI-APs) was determined by staining cells with Alexa 488-conjugated inactivated aerolysin [fluorescently-labeled inactive toxin aerolysin (FLAER); Protox Biotech, Victoria, BC, Canada] and appropriate primary antibodies: mouse anti-decay accelerating factor (DAF; IA10), −CD16 (3G8), −CD24 (ML5), −CD59 (5H8), and −CD48 (BJ40) followed by a PE-conjugated anti-mouse IgG antibody (3G8, ML5, BJ40, and secondary antibodies; BD Biosciences, Franklin Lakes, NJ). Cells were analyzed by flow cytometry (Cant II; BD Biosciences) with Flowjo software (v9.5.3, Tommy Digital, Tokyo, Japan).

Functional analysis in HEK293 cells

PIGN-knockout cells were generated from HEK293 cells using the CRISPR/Cas System [10]. We obtained the human codon-optimized *Streptococcus pyogenes* Cas9 and chimeric guide RNA expression plasmid pX330 from Addgene (Cambridge, MA). The seed sequence for the SpCas9 target site in *PIGN* exon 4 (CCA-GGTCATGTAGCTCTGATAGC) was selected and a pair of annealed oligos designed according to this sequence and cloned into the *Bbs* I sites of pX330. HEK293 cells were transfected with pX330 containing the target site using Lipofectamine 2000 (Invitrogen, Carlsbad, CA). Cells were stained with anti-CD59 antibody 14 days after transfection, and *PIGN*-knockout clones were obtained by limiting dilution.

PIGN-knockout HEK293 cells (clone PIGNKO2-12) were transiently transfected with a wild-type or mutant (S290P or exon 10 skipping) *PIGN* cDNA cloned into the SRα promoter-driven expression vector pME HA-PIGN. Restoration of the surface expression of CD59, DAF, and GPI-APs was assessed 2 days later by flow cytometry.

Results

WES detected 288 and 292 rare protein-altering and splice-site variants in patients 1 and 2, respectively. We filtered out common single nucleotide polymorphisms (SNPs) that met the following two criteria: variants showing minor allele frequencies ≥1 % in dbSNP 135 and variants found in more than two of our in-house 406 control exomes (Supplementary Table 2). All genes were surveyed for compound heterozygous or homozygous mutations consistent with an autosomal recessive trait, and only *PIGN* (GenBank accession number NM_176787.4) met this criterion, possessing compound heterozygous mutations in two patients. The missense mutation c.808T >C (p.Ser270Pro) was inherited from the patients' father, while c.963G >A is a synonymous mutation inherited from their mother but located at the last base of exon 10 (Fig. 1i). Neither of the two mutations was present in the 6,500 exomes sequenced by the National Heart, Lung, and Blood Institute exome project. In our 406 in-house control exomes, c.808T >C was absent, but c.963G >A was found in one, as a heterozygous mutation. c.808T >C occurred at evolutionary conserved amino acids (Fig. 1g) and was predicted to be pathogenic using online software (Supplementary Table 3). To examine the actual effects of c.963G >A on splicing, RT-PCR was performed (Fig. 1h, i) and a single band (200 bp) corresponding to the wild-type *PIGN* allele was amplified from control LCL cDNA template (Fig. 1h). By contrast, two aberrant faint bands were detected in addition to a wild-type band from patient cDNA (Fig. 1h). Sequencing of the upper aberrant band indicated a 53-bp insertion of intron 10 sequences that had

used a cryptic splice donor site within intron 10, producing a premature stop codon (p.Ala322Valfs*24). Sequencing of the lower band demonstrated the deletion of exon 10 from wild-type *PIGN* mRNA, also producing a premature stop codon (p.Glu308Glyfs*2). Therefore, these two mutant transcripts are likely to be degraded by nonsense-mediated mRNA decay (NMD). In fact, CHX treatment, which inhibits NMD, increased the intensity of the aberrant bands, suggesting that NMD was indeed involved.

To examine the functional impairment of *PIGN* caused by compound heterozygous mutations, the surface expression of various GPI-APs was analyzed by flow cytometry. CD16 and CD24 expression on blood granulocytes was decreased to 26–54 % of normal levels in both patients (Fig. 2a). No abnormal GPI-APs expression was observed on LCLs from either patient (Supplementary Fig. 1).

Transient expression of p.Ser270Pro and exon 10 skipping (p.Glu308Glyfs*2) mutants in *PIGN*-knockout HEK293 cells, in which expression of GPI-APs CD59 was decreased, was confirmed by immunoblotting. Expression of the exon 10 skipping mutant was decreased compared with that of wild-type and p.Ser270Pro mutant (Supplementary Fig. 2). CD59 expression was only partially or hardly restored by the transient expression of p.Ser270Pro and exon 10 skipping mutants, respectively, suggesting severe or complete loss of PIGN activity (Fig. 2b).

Discussion

Herein, we report a second family with *PIGN* mutations that showed clinical features common to a previous affected family, including congenital anomalies, developmental delay, hypotonia, and epilepsy [7]. In addition, nystagmus was an early symptom of patients in this study and was also observed in five of seven patients previously [7]. Of note, progressive cerebellar atrophy was observed in the current patient 1, and this appears to be a novel phenotype associated with *PIGN*

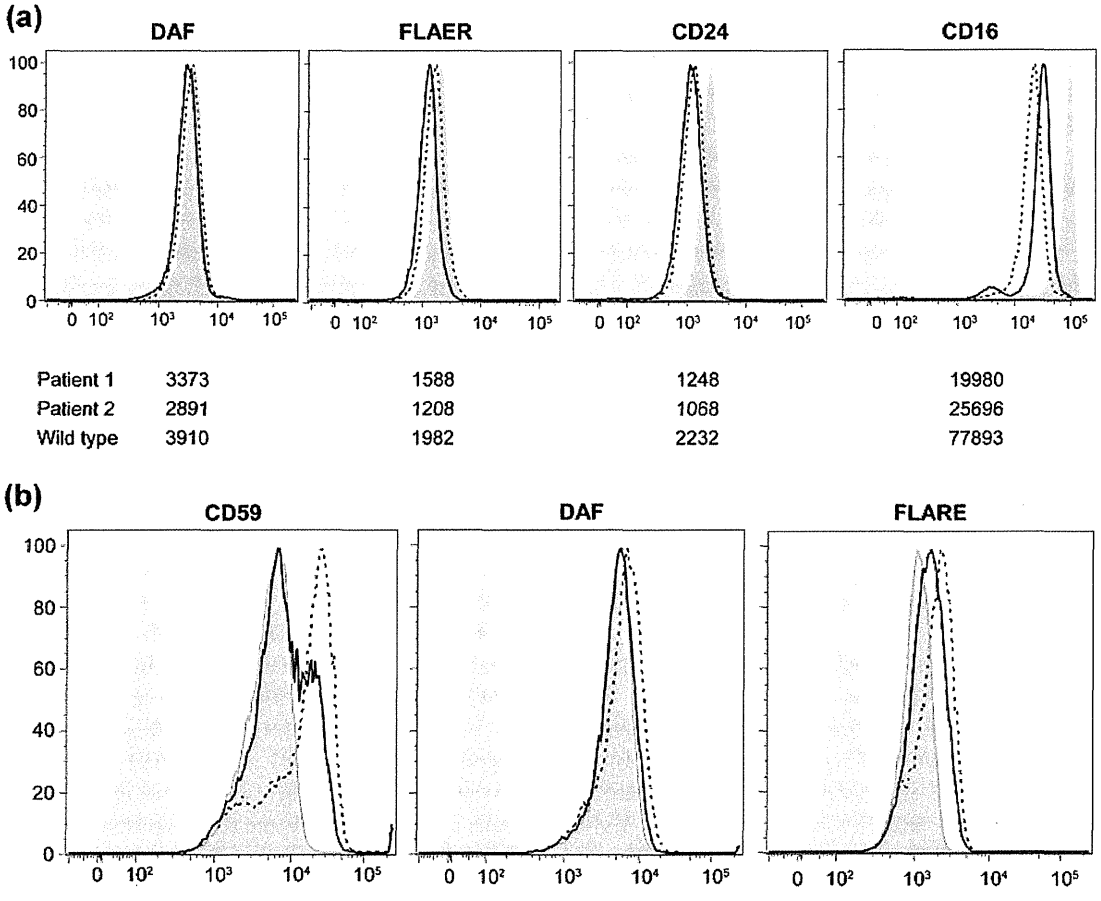

Fig. 2 **a** Surface expression of various GPI-APs on patient granulocytes (patient 1: *dotted lines*, patient 2: *solid lines*), a normal control (*dark shadow*) and an isotype control (*light shadows*). Numbers represent mean fluorescent intensities. Expression of DAF and FLAER in both patients did not significantly change compared with the control. However, CD16 and CD24 expression decreased to 26–54 % of normal levels. **b** *PIGN*-knockout HEK293 cells were transiently transfected with wild type (*dotted lines*) or mutants (exon 10 skipping: *gray line*, p.Ser270Pro: *black line*) of pME HA-PIGN vectors. Empty vector: *dark shadow*, isotype control: *light shadow*. Expression of CD59 was only partially or hardly restored by p.Ser270Pro and exon 10-skipping vectors, respectively

mutations as two patients examined by MRI showed no cerebellar atrophy but only minimal loss of vermis parenchyma in one patient (patient V-1) in the previous report [7].

PIGN is involved in the addition of phosphoethanolamine to the first mannose in GPI [6]. In *Pign*-knockout mouse F9 embryonal carcinoma cells, the first mannose in GPI precursors is not modified by phosphoethanolamine. Nevertheless, further biosynthetic steps continue and the cell surface expression of GPI-anchored proteins is only partially affected [6], suggesting that this modification may not be essential for GPI-anchored protein biosynthesis [6]. By contrast, the *gonzo* mouse line, which harbors the splice donor site mutation in *Pign*, showed abnormal forebrain development resembling holoprosencephaly [11], and patients with *PIGN* mutations show severe phenotypes such as multiple congenital anomalies, neurological impairment, and even lethality [7]; this indicates that particular defects of *PIGN*/*Pign* cause abnormal development both in mice and humans. Although the overall amount of GPI-anchored proteins might not be significantly affected by *PIGN* defects, as revealed by the minimal decrease in DAF and FLAER expression on patient granulocytes in the present study, changes to a subset of GPI-anchored proteins such as CD16 and CD24 can be sufficient to cause severe neurological phenotypes. Additionally or alternatively, GPI-APs expressed on PIGN-defective cells lack the phosphoethanolamine-side branch, and this abnormal structure of the glycan part of the anchor might affect functions of GPI-APs. Functional analysis using neuronal cells may provide novel insights into the pathogenesis of neurological phenotypes caused by *PIGN* mutations.

Seven genes (*PIGA*, *PIGM*, *PIGN*, *PIGV*, *PIGL*, *PIGO*, and *PGAP2*) have been identified as being mutated in patients with neurological abnormalities. Mutations in three of these (*PIGV*, *PIGO*, and *PGAP2*) cause hyperphosphatasia [3, 12–14], suggesting that ALP is a useful marker for suspected GPI anchor-synthesis pathway deficiencies. However, mutations of the other four genes (*PIGA*, *PIGM*, *PIGN*, and *PIGL*) did not cause hyperphosphatasia [7, 14, 15], so clinical diagnosis might be difficult in the absence of specific biomarkers. Even in clinically unsuspected patients, WES may identify mutations in genes involved in the GPI anchor-synthesis pathway. Current advances in next generation sequencing should find more comprehensive answers for unsolved GPI anchor-related diseases.

Acknowledgments We would like to thank patients and their parents for their participation in this study. We also thank Nobuko Watanabe and Kana Miyanagi for technical assistance. This work was supported by the Ministry of Health, Labour, and Welfare of Japan; a Grant-in-Aid for Scientific Research (A), (B), and (C) from the Japan Society for the Promotion of Science (A: 24249019, B: 25293085 25293235, C: 23590363); the Takeda Science Foundation; the Japan Science and Technology Agency; the Strategic Research Program for Brain Sciences (11105137); and a Grant-in-Aid for Scientific Research on Innovative Areas (Transcription Cycle, Exploring molecular basis for brain diseases based on personal genomics) from the Ministry of Education, Culture, Sports, Science, and Technology of Japan (12024421, 25129705).

References

1. Freeze HH, Eklund EA, Ng BG, Patterson MC (2012) Neurology of inherited glycosylation disorders. Lancet Neurol 11(5):453–466. doi:10.1016/s1474-4422(12)70040-6
2. Maeda Y, Kinoshita T (2011) Structural remodeling, trafficking and functions of glycosylphosphatidylinositol-anchored proteins. Prog Lipid Res 50(4):411–424. doi:10.1016/j.plipres.2011.05.002
3. Hansen L, Tawamie H, Murakami Y, Mang Y, ur Rehman S, Buchert R, Schaffer S, Muhammad S, Bak M, Nothen MM, Bennett EP, Maeda Y, Aigner M, Reis A, Kinoshita T, Tommerup N, Baig SM, Abou Jamra R (2013) Hypomorphic mutations in *PGAP2*, encoding a GPI-anchor-remodeling protein, cause autosomal-recessive intellectual disability. Am J Hum Genet 92(4):575–583. doi:10.1016/j.ajhg.2013.03.008
4. Krawitz PM, Murakami Y, Riess A, Hietala M, Kruger U, Zhu N, Kinoshita T, Mundlos S, Hecht J, Robinson PN, Horn D (2013) *PGAP2* mutations, affecting the GPI-anchor-synthesis pathway, cause hyperphosphatasia with mental retardation syndrome. Am J Hum Genet 92(4):584–589. doi:10.1016/j.ajhg.2013.03.011
5. Kvarnung M, Nilsson D, Lindstrand A, Korenke GC, Chiang SC, Blennow E, Bergmann M, Stodberg T, Makitie O, Anderlid BM, Bryceson YT, Nordenskjold M, Nordgren A (2013) A novel intellectual disability syndrome caused by GPI anchor deficiency due to homozygous mutations in *PIGT*. J Med Genet 50(8):521–528. doi:10.1136/jmedgenet-2013-101654
6. Hong Y, Maeda Y, Watanabe R, Ohishi K, Mishkind M, Riezman H, Kinoshita T (1999) Pig-n, a mammalian homologue of yeast Mcd4p, is involved in transferring phosphoethanolamine to the first mannose of the glycosylphosphatidylinositol. J Biol Chem 274(49):35099–35106
7. Maydan G, Noyman I, Har-Zahav A, Neriah ZB, Pasmanik-Chor M, Yeheskel A, Albin-Kaplanski A, Maya I, Magal N, Birk E, Simon AJ, Halevy A, Rechavi G, Shohat M, Straussberg R, Basel-Vanagaite L (2011) Multiple congenital anomalies-hypotonia-seizures syndrome is caused by a mutation in *PIGN*. J Med Genet 48(6):383–389. doi:10.1136/jmg.2010.087114
8. Saitsu H, Nishimura T, Muramatsu K, Kodera H, Kumada S, Sugai K, Kasai-Yoshida E, Sawaura N, Nishida H, Hoshino A, Ryujin F, Yoshioka S, Nishiyama K, Kondo Y, Tsurusaki Y, Nakashima M, Miyake N, Arakawa H, Kato M, Mizushima N, Matsumoto N (2013) *De novo* mutations in the autophagy gene *WDR45* cause static encephalopathy of childhood with neurodegeneration in adulthood. Nat Genet. doi:10.1038/ng.2562
9. Saitsu H, Kato M, Okada I, Orii KE, Higuchi T, Hoshino H, Kubota M, Arai H, Tagawa T, Kimura S, Sudo A, Miyama S, Takami Y, Watanabe T, Nishimura A, Nishiyama K, Miyake N, Wada T, Osaka H, Kondo N, Hayasaka K, Matsumoto N (2010) *STXBP1* mutations in early infantile epileptic encephalopathy with suppression-burst pattern. Epilepsia 51(12):2397–2405. doi:10.1111/j.1528-1167.2010.02728.x
10. Cong L, Ran FA, Cox D, Lin S, Barretto R, Habib N, Hsu PD, Wu X, Jiang W, Marraffini LA, Zhang F (2013) Multiplex genome engineering using CRISPR/Cas systems. Science 339(6121):819–823. doi:10.1126/science.1231143
11. McKean DM, Niswander L (2012) Defects in GPI biosynthesis perturb Cripto signaling during forebrain development in two new mouse models of holoprosencephaly. Biology open 1(9):874–883. doi:10.1242/bio.20121982
12. Freeze HH (2013) Understanding human glycosylation disorders: biochemistry leads the charge. J Biol Chem 288(10):6936–6945. doi:10.1074/jbc.R112.429274

13. Krawitz PM, Murakami Y, Hecht J, Kruger U, Holder SE, Mortier GR, Delle Chiaie B, De Baere E, Thompson MD, Roscioli T, Kielbasa S, Kinoshita T, Mundlos S, Robinson PN, Horn D (2012) Mutations in *PIGO*, a member of the GPI-anchor-synthesis pathway, cause hyperphosphatasia with mental retardation. Am J Hum Genet 91(1):146–151. doi:10.1016/j.ajhg.2012.05.004
14. Almeida AM, Murakami Y, Layton DM, Hillmen P, Sellick GS, Maeda Y, Richards S, Patterson S, Kotsianidis I, Mollica L, Crawford DH, Baker A, Ferguson M, Roberts I, Houlston R, Kinoshita T, Karadimitris A (2006) Hypomorphic promoter mutation in *PIGM* causes inherited glycosylphosphatidylinositol deficiency. Nat Med 12(7):846–851. doi:10.1038/nm1410
15. Johnston JJ, Gropman AL, Sapp JC, Teer JK, Martin JM, Liu CF, Yuan X, Ye Z, Cheng L, Brodsky RA, Biesecker LG (2012) The phenotype of a germline mutation in *PIGA*: the gene somatically mutated in paroxysmal nocturnal hemoglobinuria. Am J Hum Genet 90(2):295–300. doi:10.1016/j.ajhg.2011.11.031

RESEARCH ARTICLE

Human Mutation

OFFICIAL JOURNAL
HGVS
HUMAN GENOME VARIATION SOCIETY
www.hgvs.org

De Novo Mutations in *SLC35A2* Encoding a UDP-Galactose Transporter Cause Early-Onset Epileptic Encephalopathy

Hirofumi Kodera,[1†] Kazuyuki Nakamura,[1,2†] Hitoshi Osaka,[3] Yoshihiro Maegaki,[4] Kazuhiro Haginoya,[5,6] Shuji Mizumoto,[7] Mitsuhiro Kato,[2] Nobuhiko Okamoto,[8] Mizue Iai,[3] Yukiko Kondo,[1] Kiyomi Nishiyama,[1] Yoshinori Tsurusaki,[1] Mitsuko Nakashima,[1] Noriko Miyake,[1] Kiyoshi Hayasaka,[2] Kazuyuki Sugahara,[7] Isao Yuasa,[9] Yoshinao Wada,[10] Naomichi Matsumoto,[1*] and Hirotomo Saitsu[1**]

[1]Department of Human Genetics, Yokohama City University Graduate School of Medicine, Kanazawa-ku, Yokohama 236-0004, Japan; [2]Department of Pediatrics, Yamagata University School of Medicine, Yamagata 990-9585, Japan; [3]Division of Neurology, Clinical Research Institute, Kanagawa Children's Medical Center, Minami-ku, Yokohama 232-8555, Japan; [4]Division of Child Neurology, Faculty of Medicine, Tottori University, Yonago 683-8504, Japan; [5]Department of Pediatrics, Tohoku University School of Medicine, Aoba-ku, Sendai 980-8574, Japan; [6]Department of Pediatric Neurology, Takuto Rehabilitation Center for Children, Taihaku-ku, Sendai 982-0241, Japan; [7]Laboratory of Proteoglycan Signaling and Therapeutics, Frontier Research Center for Post-Genomic Science and Technology, Graduate School of Life Science, Hokkaido University, Sapporo 001-0021, Japan; [8]Department of Medical Genetics, Osaka Medical Center and Research Institute for Maternal and Child Health, Izumi, Osaka 594-1101, Japan; [9]Division of Legal Medicine, Faculty of Medicine, Tottori University, Yonago 683-8503, Japan; [10]Department of Molecular Medicine, Osaka Medical Center and Research Institute for Maternal and Child Health, Izumi, Osaka 594-1101, Japan

Communicated by María-Jesús Sobrido

Received 16 May 2013; accepted revised manuscript 15 September 2013.
Published online 30 September 2013 in Wiley Online Library (www.wiley.com/humanmutation). DOI: 10.1002/humu.22446

ABSTRACT: Early-onset epileptic encephalopathies (EOEE) are severe neurological disorders characterized by frequent seizures accompanied by developmental regression or retardation. Whole-exome sequencing of 12 patients together with five pairs of parents and subsequent Sanger sequencing in additional 328 EOEE patients identified two de novo frameshift and one missense mutations in *SLC35A2* at Xp11.23, respectively. The three patients are all females. X-inactivation analysis of blood leukocyte DNA and mRNA analysis using lymphoblastoid cells derived from two patients with a frameshift mutation indicated that only the wild-type *SLC35A2* allele was expressed in these cell types, at least in part likely as a consequence of skewed X-inactivation. *SLC35A2* encodes a UDP-galactose transporter (UGT), which selectively supplies UDP-galactose from the cytosol to the Golgi lumen. Transient expression experiments revealed that the missense mutant protein was correctly localized in the Golgi apparatus. In contrast, the two frameshift mutant proteins were not properly expressed, suggesting that their function is severely impaired. Defects in the UGT can cause congenital disorders of glycosylation. Of note, no abnormalities of glycosylation were observed in three serum glycoproteins, which is consistent with favorably skewed X-inactivation. We hypothesize that a substantial number of neurons might express the mutant *SLC35A2* allele and suffer from defective galactosylation, resulting in EOEE.
Hum Mutat 34:1708–1714, 2013. © 2013 Wiley Periodicals, Inc.

KEY WORDS: early-onset epileptic encephalopathy; *SLC35A2*; congenital disorders of glycosylation

Introduction

Glycosylation is the process of adding complex sugar chains (glycans) to proteins and lipids. Protein glycosylation includes *N*-linked and *O*-linked glycosylation pathways in the endoplasmic reticulum (ER)–Golgi network [Freeze, 2013]. To enable glycan biosynthesis, monosaccharides in the form of nucleotide sugars, such as GDP-fucose, CMP-sialic acid, and UDP-galactose, must be delivered into the lumen of the ER and Golgi apparatus by their respective nucleotide-sugar transporters [Liu et al., 2010]. Defects of the glycosylation process cause congenital disorders of glycosylation (CDG). To date, nearly 70 CDG have been identified, most caused by either the *N*-linked or *O*-linked glycosylation pathway, or both [Freeze, 2013; Jaeken and Matthijs, 2007]. Because glycosylation is a ubiquitous cellular process, its defects affect multiple organ systems with various features, accompanied by facial dysmorphism. The central nervous system is one of the most often affected organs, frequently resulting in structural abnormalities, developmental delay, and epileptic seizures [Freeze et al., 2012].

Additional Supporting Information may be found in the online version of this article.

†These authors contributed equally to this work.

*Correspondence to: Naomichi Matsumoto. Department of Human Genetics, Yokohama City University Graduate School of Medicine, 3-9 Fukuura, Kanazawa-ku, Yokohama 236-0004, Japan. E-mail: naomat@yokohama-cu.ac.jp

**Correspondence to: Hirotomo Saitsu. Department of Human Genetics, Yokohama City University Graduate School of Medicine, 3-9 Fukuura, Kanazawa-ku, Yokohama 236-0004, Japan. E-mail: hsaitsu@yokohama-cu.ac.jp

Contract grant sponsors: Ministry of Health, Labour, and Welfare of Japan; the Japan Society for the Promotion of Science (Grant-in-Aid for Scientific Research B [25293085], [25293235], Grant-in-Aid for Scientific Research A [13313587]); Takeda Science Foundation; Japan Science and Technology Agency; Strategic Research Program for Brain Sciences (11105137); Grants-in-Aid for Scientific Research on Innovative Areas (Transcription Cycle, Neuroglycobiology) from the Ministry of Education, Culture, Sports, Science, and Technology of Japan (12024421, 24110501).

Early-onset epileptic encephalopathies (EOEE), with onset before 1 year of age, are characterized by severe seizures (often). infantile spasms), frequent interictal epileptiform activity on a disorganized electroencephalogram (EEG) background, and developmental regression or retardation [Holland and Hallinan, 2010]. Ohtahara syndrome (MIMs # 308350, 612164), West syndrome (WS; MIMs # 308350, 300672, 612164), early myoclonic epileptic encephalopathy (MIM #609304), malignant migrating partial seizures of infancy (MIM #614959), and Dravet syndrome (MIM #607208) are the best known epileptic encephalopathies recognized by the International League Against Epilepsy. However, many infants with these syndromes do not strictly fit within the electroclinical parameters of these syndromes. Recently, several causative genes have been reported in patients both with well-recognized and unclassified EOEE syndromes: *ARX* (MIM #300382), *CDKL5* (MIM #300203), *STXBP1* (MIM #602926), *SLC25A22* (MIM #609302), *SCN1A* (MIM #182389), *KCNQ2* (MIM #602235), and *KCNT1* (MIM #608167) [Barcia et al., 2012; Claes et al., 2001; Kalscheuer et al., 2003; Kato et al., 2007; Molinari et al., 2005; Saitsu et al., 2008, 2012a; Stromme et al., 2002; Weckhuysen et al., 2012]. These genes encode sodium or potassium channels, transcription factors, a mitochondrial glutamate transporter, and a regulator of neurotransmitter release, and are able to explain part of the genetic cause of EOEE. Because epileptic seizures are one of the main symptoms with CDG, abnormal glycosylation may be found in EOEE. In fact, de novo mutations in *SLC35A2* (MIM #314375), encoding a UDP-galactose transporter (UGT), have recently been reported in three patients with CDG (one female with a heterozygous mutation and two males with a mosaic mutation), and two of them showed seizures and hypsarrhythmia on EEG, suggesting WS [Ng et al., 2013]. It would be worth checking *SLC35A2* mutations in a large cohort of patients with EOEE.

In this study, whole-exome sequencing (WES) of 12 patients together with five pairs of parents (five trios) and subsequent Sanger sequencing in additional 328 patients with EOEE identified two de novo frameshift and one de novo missense mutations in *SLC35A2*, respectively, confirming that de novo *SLC35A2* mutations are one of the genetic causes for EOEE.

Materials and Methods

Methods for RNA analysis, X-inactivation analysis, and mass spectrometry are described in the Supp. Methods.

Patients

A total of 328 patients with EOEE (67 patients with Ohtahara syndrome, 150 with WS, and 111 with unclassified EOEE) were analyzed for *SLC35A2* mutations. The diagnosis was made based on clinical features and characteristic patterns on EEG. In 257 patients, mutations in *STXBP1* and *KCNQ2* had been excluded by high-resolution melting analysis in advance. Experimental protocols were approved by the Institutional Review Board of Yokohama City University School of Medicine. Clinical information and peripheral blood samples were obtained from the family members after obtaining written informed consent.

Exome Sequencing

WES for 12 patients with EOEE, in whom initial diagnosis was Ohtahara syndrome, had been previously performed [Saitsu et al., 2012a, 2012b]. In this study, we additionally analyzed parental samples from five patients by WES. Genomic DNA was captured using the SureSelectXT Human All Exon v4 Kit (Agilent Technologies, Santa Clara, CA) and sequenced with four samples per lane on an Illumina HiSeq 2000 (Illumina, San Diego, CA) with 101-bp paired-end reads. Image analysis and base calling were performed by sequence control software with real-time analysis and CASAVA software v1.8 (Illumina). Exome data processing, variant calling, and variant annotation were performed as previously described [DePristo et al., 2011; Saitsu et al., 2013; Wang et al., 2010]. All de novo candidate mutations detected by WES were confirmed by Sanger sequencing.

Mutation Screening

Genomic DNA was amplified using an illustra GenomiPhi V2 DNA Amplification Kit (GE Healthcare, Buckinghamshire, UK). Exons 1–5 covering the *SLC35A2* coding region of two transcript variants (transcript variant 1, GenBank accession number NM_005660.1, encoding UGT2; transcript variant 3, GenBank accession number NM_001042498.2, encoding UGT1) were screened by Sanger sequencing. PCR primers and conditions are available on request. All novel mutations were verified using original genomic DNA, and searched for in the variant database of our 408 in-house control exomes.

Expression Vectors

Total RNA from lymphoblastoid cells was reverse transcribed using the PrimeScript 1st strand synthesis kit with random hexamers (Takara, Ohtsu, Japan) as previously reported [Saitsu et al., 2010]. The following primers were used to isolate full-length human *SLC35A2* cDNA (amino acids 1–393, GenBank accession number NM_001042498.2): forward 5′-GGAATTCAGATGCCAACATGGCAGCGGTTGG–3′ and reverse 5′-GGCTCGAGATTGCTGCCAGCCCTCACTTCAC–3′. *SLC35A2* cDNA was inserted into pBlueScript SK(–) vector (Agilent Technologies), and site-directed mutagenesis was performed using a KOD-Plus-Mutagenesis kit (Toyobo, Osaka, Japan) according to the manufacturer's protocol to generate *SLC35A2* mutants including c.433_434del (p.Tyr145Profs*76), c.972del (p.Phe324Leufs*25), and c.638C>T (p.Ser213Phe). Subsequently, mutant *SLC35A2* cDNAs that excluded termination codons were amplified by PCR, inserted into pEF6/V5-His C vector (Life Technologies Co., Carlsbad, CA) to generate C terminal V5-epitope tag. All variant cDNAs were confirmed by Sanger sequencing.

Cell Culture

Mouse neuroblastoma 2A (N2A) cells were cultured at 37°C under 5% CO_2 in DMEM, high glucose, GlutaMAX(™) supplemented with 10% fetal bovine serum and Penicillin–Streptomycin (Life Technologies Co.).

Immunofluorescence Microscopy

N2A cells on glass cover slips were transfected with 200 ng of plasmid DNA using X-tremeGENE 9 DNA Transfection Reagent (Roche Diagnostics, Mannheim, Germany). After 24 hr, cells were fixed in 4% paraformaldehyde/PBS for 15 min and permeabilized in 0.1% Triton X-100/PBS for 5 min. Cells were then blocked with 10% normal goat serum for 30 min. V5-tagged UGT1 were detected by mouse anti-V5 antibody (1:200 dilution; Life Technologies) and Alexa-488-conjugated goat anti-mouse immunoglobulin G (1:1000 dilution; Life Technologies). Cover slips were mounted using

Vectashield (Vector Laboratories, Youngstown, OH) that contained 4′,6-diamidino-2-phenylindole (DAPI) and visualized with an inverted FV1000-D confocal microscope (Olympus, Tokyo, Japan).

Results

To systemically screen de novo or recessive mutations, we conducted trio-based WES in five patients with EOEE. None of the recessive mutations in known EOEE genes were found in WES data (*SLC25A22*, *PNPO*; MIM #610090, *PNKP*; MIM #613402, *PLCB1*; MIM #613722, and *ST3GAL3*; MIM #615006) [Hu et al., 2011; Kurian et al., 2010; Mills et al., 2005; Molinari et al., 2005; Shen et al., 2010]. Instead, we found one or two de novo nonsynonymous mutations in each of the five trios (Supp. Table S1). Among them, a sole de novo frameshift mutation in *SLC35A2* at Xp11.23 was found in two patients: c.433_434del (p.Tyr145Profs*76) in patient 1 and c.972del (p.Phe324Leufs*25) in patient 2, which were confirmed by Sanger sequencing. No *SLC35A2* mutation was found in the other seven patients analyzed by WES. However, subsequent *SLC35A2* mutation analysis by Sanger sequencing in a cohort of 328 patients with EOEE revealed another de novo missense mutation (c.638C>T [p.Ser213Phe]) in patient 3 (Fig. 1A). None of the three mutations was found in the 6,500 National Heart, Lung, and Blood Institute exomes (http://evs.gs.washington.edu/EVS/) or our 408 in-house control exomes. All patients with a *SLC35A2* mutation are female.

As human female cells are subject to X-chromosome inactivation, we examined the X-inactivation pattern using a fragile X mental retardation locus methylation assay and human androgen receptor assay on genomic DNA from peripheral leukocytes [Kondo et al., 2012]. A markedly skewed pattern was observed in patients 1 and 2 (noninformative in patient 3) (Supp. Table S2). Reverse-transcription PCR and sequencing of total RNA extracted from lymphoblastoid cell lines derived from patients 1 and 2 revealed that only the wild-type (WT) *SLC35A2* allele was expressed, suggesting that the mutant alleles underwent X-inactivation, though degradation of mutant transcripts by nonsense-mediated mRNA decay may be involved (Supp. Fig. S1). Cells from patient 3 were unavailable. It is unknown whether the mutant allele undergoes similar X-inactivation in brain tissues.

SLC35A2 encodes a UGT, which selectively supplies UDP-galactose from the cytosol to the Golgi lumen [Ishida et al., 1996; Miura et al., 1996]. Two human UGT splice variants have been studied: UGT1 encoded by transcript variant 3 (NM_001042498.2) and UGT2 by transcript variant 1 (NM_005660.1) [Ishida et al., 1996; Kabuss et al., 2005; Miura et al., 1996], both of which are predicted to have a 10-transmembrane domain and differ only at the carboxyl-terminal five or eight amino acid residues (Fig. 1B) [Kabuss et al., 2005; Miura et al., 1996]. The three mutations would affect both UGT1 and UGT2. Two mutations (p.Tyr145Profs*76 and p.Phe324Leufs*25) would cause truncation of UGT within the transmembrane domain, and the missense mutation (p.Ser213Phe) occurs at an evolutionarily conserved amino acid (Fig. 1B and Supp. Fig. S2). To examine the effect of the three *SLC35A2* mutations, we performed transient expression experiments in N2A cells. C-terminally V5 epitope-tagged WT UGT1 was localized to the Golgi apparatus, similar to endogenous UGT1 [Yoshioka et al., 1997]. The p.Ser213Phe mutant showed a similar expression pattern to

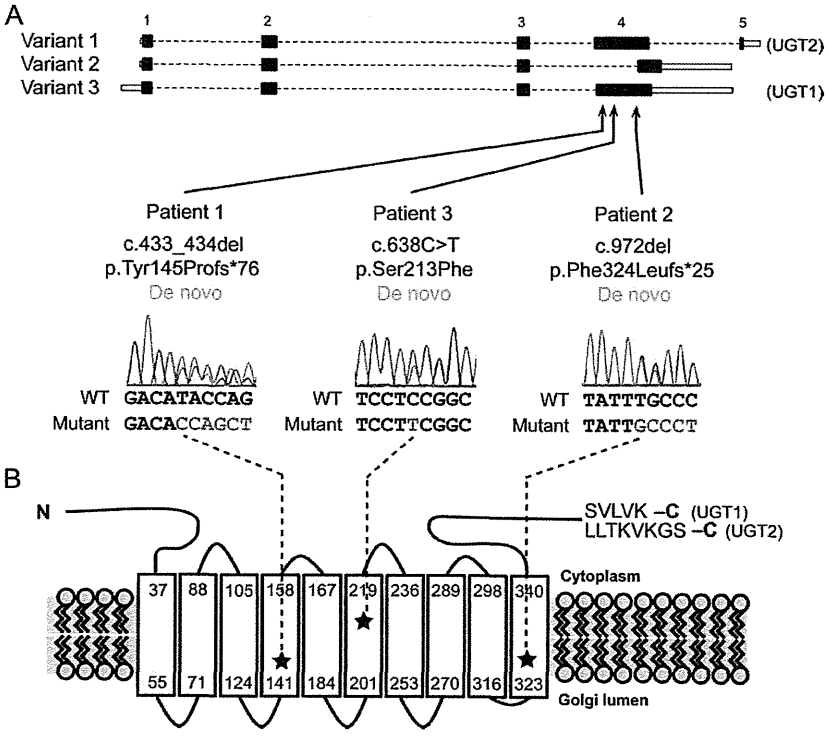

Figure 1. De novo *SLC35A2* mutations in EOEE patients. **A:** Schematic representation of *SLC35A2* (open and filled rectangles represent untranslated regions and coding regions, respectively). There are three transcript variants: variant 1 (GenBank accession number, NM_005660.1) encoding UGT2, variant 2 (NM_005660.1), and variant 3 (NM_001042498.2) encoding UGT1. The three de novo mutations occurred in both variants 1 and 3, but not in variant 2. **B:** Topological prediction of UGT1 and UGT2 proteins [Kabuss et al., 2005]. The three mutations (stars) are predicted to be localized in the transmembrane domains. The C-terminal five amino acids (SVLVK) in UGT1 are replaced by eight amino acids (LLTKVKGS) in UGT2. *SLC35A2* variants were deposited in a gene-specific database (http://databases.lovd.nl/shared/genes/SLC35A2).

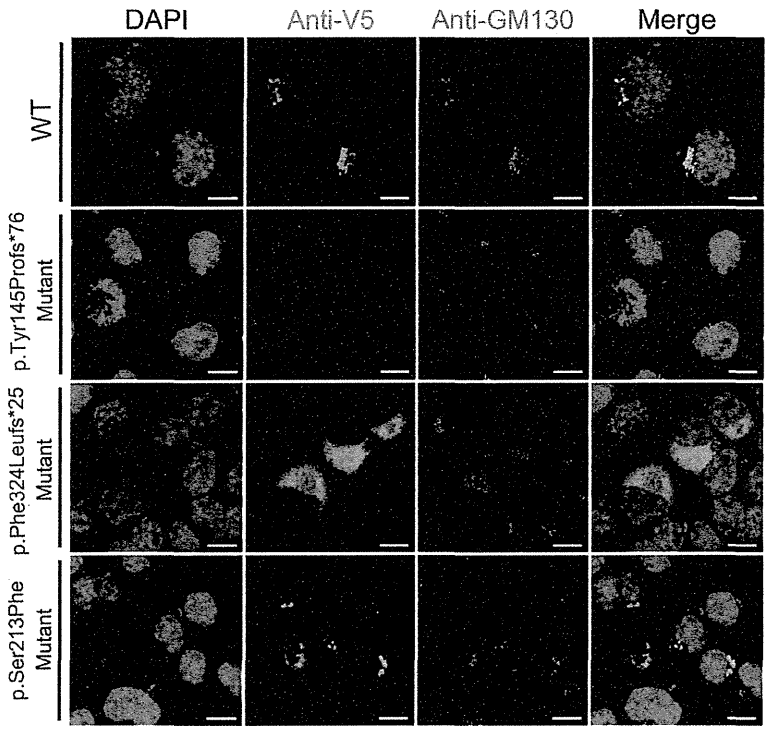

Figure 2. Expression of V5-tagged UGT1 proteins in N2A cells. Expression of WT and the three mutant UGT1 proteins in N2A cells. V5-tagged WT UGT1 (top, green) and the p.Ser213Phe mutant (bottom, green) colocalized with the Golgi marker GM130 (red), suggesting localization to the Golgi apparatus similar to endogenous UGT1. In contrast, the p.Phe324Leufs*25 mutant (lower middle, green) was expressed in the cytosolic compartment, and expression of the p.Tyr145Profs*76 mutant (upper middle, green) was severely diminished. The nucleus was stained with DAPI (blue). The scale bars represent 10 μm.

the WT. In contrast, the p.Phe324Leufs*25 mutant was expressed in the cytosolic compartment and expression of the p.Tyr145Profs*76 mutant was severely diminished, suggesting that the function of the two truncated UGT1 proteins would be severely impaired (Fig. 2).

Because nucleotide-sugar transporters including UGT are critical components of glycosylation pathways such as *N*-glycosylation and *O*-glycosylation in eukaryotes, functional aberration of UGT is likely to affect protein glycosylation [Jaeken, 2003; Liu et al., 2010; Muntoni, 2004; Wopereis et al., 2006]. Therefore, we investigated glycosylation of serum glycoproteins isolated from the patients with a *SLC35A2* mutation, by isoelectric focusing, electrospray ionization, and matrix-assisted laser desorption/ionization mass spectrometry (MALDI-MS) of transferrin and apolipoprotein CIII, and by MALDI-MS of immunoglobulin G (Supp. Figs. S3–S5 and Supp. Table S3). However, we could not detect any abnormalities of *N*-glycosylation or *O*-glycosylation in these serum glycoproteins. Considering that only WT *SLC35A2* is expressed in lymphoblastoid cells from the two patients, these normal glycosylation profiles of serum glycoproteins may be reasonable.

The clinical features of patients with a *SLC35A2* mutation are presented in Table 1. Dysmorphological findings such as thick eyebrows, a broad nasal bridge, thick lips, and maxillary prognathism were found (Fig. 3A–C). Brain magnetic resonance imaging (MRI) showed cerebral and cerebellar atrophy and thinning of the corpus callosum in two patients, 1 and 3, an arachnoid pouch in patient 1, and an enlarged left lateral ventricle in patient 2 (Fig. 3D–H). All patients were diagnosed as WS in their clinical course, and showed no abnormalities in the skin, coagulation, or hepatic enzymes, which are often observed in patients with CDG [Freeze, 2006; Freeze et al., 2012]. On interictal EEG at 8 days after birth, patient 1 revealed brief tonic seizures of the upper extremities and a diffuse spike or sharp and slow-wave complex, which were accompanied by brief suppression for 1–2 sec (Fig. 3I). At 50 days, she showed a series of spasms, and the EEG transited to hypsarrhythmia at 2 months, leading to a diagnosis of WS. The administration of adrenocorticotropic hormone (ACTH), zonisamide, and valproic acid (VPA) was temporarily effective; however, she developed seizures again at 4 months. Seizures were refractory to vitamin B6, phenobarbital, clobazam, corpus callosotomy, or a ketogenic diet. At 8 years of age, she showed hypotonia, severe intellectual disability, motor developmental delay, no head control, and no meaningful words. Patient 2 developed a series of spasms, and showed a diffuse spike or sharp and slow-wave complex on interictal EEG at 1 month. EEG transited to hypsarrhythmia at 4 months, leading to a diagnosis of WS. Her seizures were temporarily controlled by combined administration of VPA, nitrazepam, and ACTH, followed by low-dose ACTH therapy; however, spasms with clustering developed again at 6 years and 6 months. At 12 years, her spasms changed into focal seizures after administration of levetiracetam, and interictal EEG showed mainly slow waves with focal spikes. She could crawl on hands and knees and had severe intellectual disability with no meaningful words. Patient 3 started to have clusters of spasms at 3 months of age, and interictal EEG during sleep revealed hypsarrhythmia, leading to a diagnosis of early-onset WS (Fig. 3J). Vitamin B6 and VPA were ineffective at treating the spasms. Subsequent treatment with ACTH eliminated her spasms and hypsarrhythmia on EEG, but brief tonic seizures without clustering relapsed 1 month after the treatment. Despite the administration of various antiepileptic drugs

Table 1. Clinical Features of Patients with a *SLC35A2* Mutation

	Patient 1	Patient 2	Patient 3
Age	8 years 10 months	12 years 8 months	10 years 5 months
Gender	Female	Female	Female
Mutation	c.433_434del (p.Tyr145Profs*76)	c.972del (p.Phe324Leufs*25)	c.638C>T (p.Ser213Phe)
Diagnosis	EOEE → West syndrome	EOEE → West syndrome	Early-onset West syndrome
Initial symptom	Tonic seizure at 6 days	Spasms at 1 month	Spasms at 3 months
Initial EEG findings	Diffuse spike or sharp and slow-wave complex with brief suppression	Diffuse sharp or spike and slow-wave complex	Hypsarrhythmia
Transition of seizures	Spasms at 50 days, tonic seizure of upper extremities at 1 year 3 months	Generalized tonic seizure and spasm at 7 months, spasm at 6 years 6 months, focal seizure at 12 years	Brief tonic seizure, spasm at 1 year 6 months
Transition of EEG findings	Hypsarrhythmia at 2 months, multifocal spikes at 2 years	Hypsarrhythmia at 4 months, diffuse fast waves at 12 years	Multifocal spike and slow wave complex at 10 months
Seizure control	Intractable	Intractable	Intractable
Development	No head control, no words at 8 years	Crawling on hand and knees, no words at 12 years	No head control, no words at 10 years
Magnetic resonance imaging findings	Arachnoid pouch at 2 months, cerebral and cerebellar atrophy, thin corpus callosum, delayed myelination at 2 years	Normal at 2 months, spotty high-intensity signal in white matter, slight enlargement of left lateral ventricle at 4 years	Normal at 3 months, severe cortical atrophy, cerebellar atrophy, thin corpus callosum at 8 years
Craniofacial findings			
Coarse face	+	+	+
Thick eyebrows	+	+	+
Broad nasal bridge	+	+	+
Thick lips	+	+	+
Semi-open mouth	+	+	+
Prominent cupid's bow	–	+	+
Epicanthal folds	–	+	+
Short philtrum	–	+	+
Maxillary prognathism	+	+	+
Full cheek	–	–	+
Other	Fused tooth	High-arched palate	Enamel hypoplasia
Blood coagulation	Normal	Normal	Normal
Skin findings	Normal	Normal	Normal
Other features	Hypotonus	White spot in the eyeground, atrial septal defect ureteropelvic junction obstruction, vesicovaginal fistula	Hypotonic quadriplegia, hipdislocation

EOEE, early-onset epileptic encephalopathy; EEG, electroencephalography.

and a ketogenic diet, daily spasms with or without clustering have persisted. At the age of 10 years, she has attained no meaningful words or head control.

Discussion

In this study, we successfully identified three de novo heterozygous mutations in *SLC35A2* in patients with EOEE. Two mutations (p.Tyr145Profs*76 and p.Phe324Leufs*25) are predicted to cause truncation of UGT, suggesting that the function of the mutant protein would be severely impaired. Consistently, transient expression of mutant proteins in N2A cells revealed that the p.Phe324Leufs*25 mutant was not localized in the Golgi apparatus and that expression of the p.Tyr145Profs*76 mutant was severely diminished. Therefore, these two frameshift mutations are likely to cause loss of function in UGT. On the other hand, the p.Ser213Phe mutant was localized in the Golgi apparatus. A single amino acid deletion of Ser213 has been reported in hamster Ugt, which is highly homologous to human UGT (see Supp. Fig. S2). The hamster mutant failed to complement the defect of UDP-galactose transport in mutant Chinese hamster ovary lec8 cells, suggesting that the Ser213 residue is essential for proper UGT function [Oelmann et al., 2001]. Thus it is possible that the p.Ser213Phe mutation causes loss of function in the UGT, though further functional studies are required for clarifying pathogenicity of this missense allele.

Mutations in three nucleotide-sugar transporters have been previously reported to cause defects in glycan biosynthesis in humans: the GDP-fucose transporter encoded by *SLC35C1*, the CMP-sialic acid transporter encoded by *SLC35A1*, and the UDP-glucuronic acid/UDP-*N*-acetylgalactosamine transporter encoded by *SLC35D1* [Hiraoka et al., 2007; Liu et al., 2010; Lubke et al., 2001; Luhn et al., 2001; Martinez-Duncker et al., 2005]. Similarly, a defect in UGT would cause UDP-galactose deficiency in the ER–Golgi network, leading to reduced galactosylation of glycoproteins, glycosphingolipids, and proteoglycans [Liu et al., 2010]. In fact, three patients with *SLC35A2* mutations have been reported in association with galactosylation-deficient serum transferrin profiles in infancy: however, they showed normal serum transferrin profiles at 3–5 years [Ng et al., 2013]. Consistent with this, our three female cases showed no glycosylation abnormalities in the three commonly assayed serum glycoproteins at 8–10 years: transferrin and apolipoprotein CIII (mainly synthesized in the liver), and immunoglobulin G (synthesized by B lymphocytes) [Goreta et al., 2012; Okanishi et al., 2008; Wada et al., 2007, 2012]. In addition, DNA extracted from the leukocytes of patients 1 and 2 showed a markedly skewed X-inactivation, and only the WT *SLC35A2* allele was expressed in lymphoblastoid cell lines from these two patients. Therefore, although the degradation of mutant transcripts is a possible explanation for selective expression of WT allele, these findings raised a possibility that liver cells and B lymphocytes expressing the mutant allele are selected against during infancy, leading to no glycosylation defects in transferrin, apolipoprotein CIII, or immunoglobulin G in three patients, with a markedly skewed X-inactivation pattern in peripheral leukocytes.

The clinical features of the patients with a *SLC35A2* mutation seemed to be consistent with the negative selection of cells expressing the mutant allele. Specific skin features, coagulopathies,

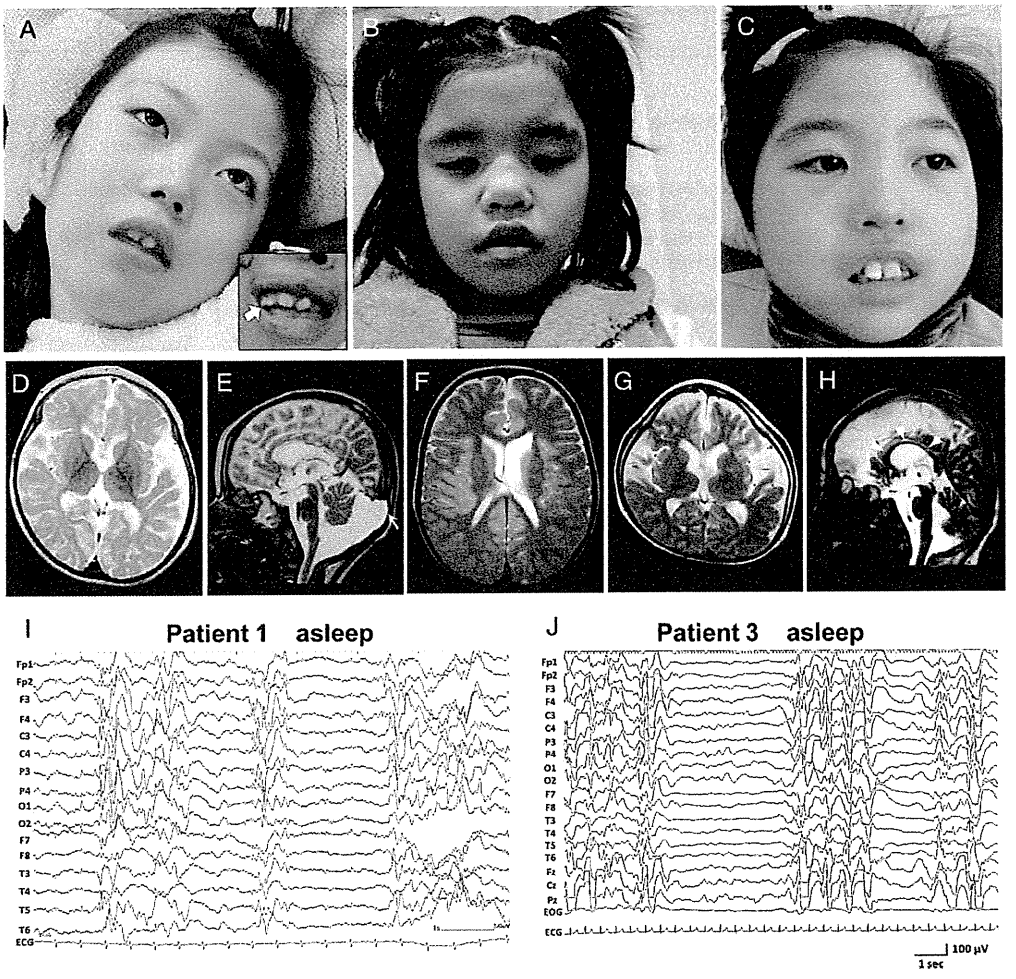

Figure 3. Facial appearance, brain (MRI), and EEG of the three patients with a *SLC35A2* mutation. **A–C:** Photograph of patient 1 at 8 years of age (**A**), patient 2 at 12 years of age (**B**), and patient 3 at 10 years of age (**C**). Note the broad nasal bridge, thick eyebrows, thick lips, semi-open mouth, and maxillary prognathism that are common in these three patients. A fused tooth observed in patient 1 is indicated by an arrow (**A**, inset). **D** and **E:** T2-weighted MRI of patient 1 at 2 years and 4 months after corpus callosotomy showed cerebral atrophy on an axial image (**D**), and cerebellar atrophy and an arachnoid pouch (white arrow) on a sagittal image (**E**). **F:** A T2-weighted axial image of patient 2 at 4 years and 3 months showed slight enlargement of the left lateral ventricle. **G** and **H:** T2-weighted MRI of patient 3 at 7 years showed cerebral atrophy with frontal lobe predominance on an axial image (**G**), and cerebellar atrophy and a thin corpus callosum (white arrowheads) on a sagittal image (**H**). **I:** Interictal EEG of patient 1 during sleep at 1.5 months old showing diffuse spike or sharp and slow-wave complexes, which were accompanied by brief suppression for 1–2 sec. **J:** Interictal EEG of patient 3 during sleep at 3 months old showing hypsarrhythmia.

immune dysfunction, cardiomyopathy, and renal dysfunction, which are often observed in glycosylation disorders [Freeze et al., 2012], were not found in these three patients, although they did present epileptic seizures (EOEE). Thus, it can be hypothesized that cells expressing the mutant allele were excluded in most organs but not the central nervous system, where a substantial number of neurons might express the mutant *SLC35A2* allele and suffer from defective galactosylation of glycoproteins, glycosphingolipids, and proteoglycans.

Together with a recent report [Ng et al., 2013], our data suggest that abnormal glycosylation may be one of the underlying pathologies of EOEE. In the absence of glycosylation abnormalities, similar to our three cases, a UGT disorder can only be diagnosed by the identification of a *SLC35A2* mutation. Recent progress in massively parallel DNA sequencing in combination with whole-exome capturing (WES) has facilitated rapid mutation detection in most exons [Bamshad et al., 2011]. WES is expected to be useful for genetic testing in EOEE, and is likely to reveal contributions from hitherto unexpected genes.

Conclusion

We identified de novo heterozygous mutations in the X-linked *SLC35A2* gene, which encodes the UGT, in patients with EOEE. Our data confirmed that abnormal glycosylation is one of the pathological features of EOEE.

Acknowledgments

The authors would like to thank all patients and their families for their participation in this study. We also thank Aya Narita and Nobuko Watanabe for technical assistance.

Disclosure statement: The authors declare no conflicts of interest.

References

Bamshad MJ, Ng SB, Bigham AW, Tabor HK, Emond MJ, Nickerson DA, Shendure J. 2011. Exome sequencing as a tool for Mendelian disease gene discovery. Nat Rev Genet 12:745–755.

Barcia G, Fleming MR, Deligniere A, Gazula VR, Brown MR, Langouet M, Chen H, Kronengold J, Abhyankar A, Cilio R, Nitschke P, Kaminska A, et al. 2012. *De novo* gain-of-function *KCNT1* channel mutations cause malignant migrating partial seizures of infancy. Nat Genet 44:1255–1259.

Claes L, Del-Favero J, Ceulemans B, Lagae L, Van Broeckhoven C, De Jonghe P. 2001. De novo mutations in the sodium-channel gene *SCN1A* cause severe myoclonic epilepsy of infancy. Am J Hum Genet 68:1327–32.

DePristo MA, Banks E, Poplin R, Garimella KV, Maguire JR, Hartl C, Philippakis AA, del Angel G, Rivas MA, Hanna M, McKenna A, Fennell TJ, et al. 2011. A framework for variation discovery and genotyping using next-generation DNA sequencing data. Nat Genet 43:491–498.

Freeze HH. 2006. Genetic defects in the human glycome. Nat Rev Genet 7:537–551.

Freeze HH. 2013. Understanding human glycosylation disorders: biochemistry leads the charge. J Biol Chem 288:6936–6945.

Freeze HH, Eklund EA, Ng BG, Patterson MC. 2012. Neurology of inherited glycosylation disorders. Lancet Neurol 11:453–466.

Goreta SS, Dabelic S, Dumic J. 2012. Insights into complexity of congenital disorders of glycosylation. Biochem Med (Zagreb) 22:156–170.

Hiraoka S, Furuichi T, Nishimura G, Shibata S, Yanagishita M, Rimoin DL, Superti-Furga A, Nikkels PG, Ogawa M, Katsuyama K, Toyoda H, Kinoshita-Toyoda A, et al. 2007. Nucleotide-sugar transporter SLC35D1 is critical to chondroitin sulfate synthesis in cartilage and skeletal development in mouse and human. Nat Med 13:1363–1367.

Holland KD, Hallinan BE. 2010. What causes epileptic encephalopathy in infancy?: the answer may lie in our genes. Neurology 75:1132–1133.

Hu H, Eggers K, Chen W, Garshasbi M, Motazacker MM, Wrogemann K, Kahrizi K, Tzschach A, Hosseini M, Bahman I, Hucho T, Mühlenhoff M, et al. 2011. *ST3GAL3* mutations impair the development of higher cognitive functions. Am J Hum Genet 89:407–414.

Ishida N, Miura N, Yoshioka S, Kawakita M. 1996. Molecular cloning and characterization of a novel isoform of the human UDP-galactose transporter, and of related complementary DNAs belonging to the nucleotide-sugar transporter gene family. J Biochem 120:1074–1078.

Jaeken J. 2003. Komrower Lecture. Congenital disorders of glycosylation (CDG): it's all in it! J Inherit Metab Dis 26:99–118.

Jaeken J, Matthijs G. 2007. Congenital disorders of glycosylation: a rapidly expanding disease family. Annu Rev Genomics Hum Genet 8:261–278.

Kabuss R, Ashikov A, Oelmann S, Gerardy-Schahn R, Bakker H. 2005. Endoplasmic reticulum retention of the large splice variant of the UDP-galactose transporter is caused by a dilysine motif. Glycobiology 15:905–911.

Kalscheuer VM, Tao J, Donnelly A, Hollway G, Schwinger E, Kubart S, Menzel C, Hoeltzenbein M, Tommerup N, Eyre H, Harbord M, Haan E, Sutherland GR, Ropers HH, Gécz J. 2003. Disruption of the serine/threonine kinase 9 gene causes severe X-linked infantile spasms and mental retardation. Am J Hum Genet 72:1401–1411.

Kato M, Saitoh S, Kamei A, Shiraishi H, Ueda Y, Akasaka M, Tohyama J, Akasaka N, Hayasaka K. 2007. A longer polyalanine expansion mutation in the *ARX* gene causes early infantile epileptic encephalopathy with suppression-burst pattern (Ohtahara syndrome). Am J Hum Genet 81:361–366.

Kondo Y, Saitsu H, Miyamoto T, Nishiyama K, Tsurusaki Y, Doi H, Miyake N, Ryoo NK, Kim JH, Yu YS, and others. 2012. A family of oculofaciocardiodental syndrome (OFCD) with a novel BCOR mutation and genomic rearrangements involving NHS. J Hum Genet 57:197–201.

Kurian MA, Meyer E, Vassallo G, Morgan NV, Prakash N, Pasha S, Hai NA, Shuib S, Rahman F, Wassmer E, Cross JH, O'Callaghan FJ, et al. 2010. Phospholipase C beta 1 deficiency is associated with early-onset epileptic encephalopathy. Brain 133:2964–2970.

Liu L, Xu YX, Hirschberg CB. 2010. The role of nucleotide sugar transporters in development of eukaryotes. Semin Cell Dev Biol 21:600–608.

Lubke T, Marquardt T, Etzioni A, Hartmann E, von Figura K, Korner C. 2001. Complementation cloning identifies CDG-IIc, a new type of congenital disorders of glycosylation, as a GDP-fucose transporter deficiency. Nat Genet 28:73–76.

Luhn K, Wild MK, Eckhardt M, Gerardy-Schahn R, Vestweber D. 2001. The gene defective in leukocyte adhesion deficiency II encodes a putative GDP-fucose transporter. Nat Genet 28:69–72.

Martinez-Duncker I, Dupre T, Piller V, Piller F, Candelier JJ, Trichet C, Tchernia G, Oriol R, Mollicone R. 2005. Genetic complementation reveals a novel human congenital disorder of glycosylation of type II, due to inactivation of the Golgi CMP-sialic acid transporter. Blood 105:2671–2676.

Mills PB, Surtees RA, Champion MP, Beesley CE, Dalton N, Scambler PJ, Heales SJ, Briddon A, Scheimberg I, Hoffmann GF, Zschocke J, Clayton PT. 2005. Neonatal epileptic encephalopathy caused by mutations in the *PNPO* gene encoding pyridox(am)ine 5′-phosphate oxidase. Hum Mol Genet 14:1077–1086.

Miura N, Ishida N, Hoshino M, Yamauchi M, Hara T, Ayusawa D, Kawakita M. 1996. Human UDP-galactose translocator: molecular cloning of a complementary DNA that complements the genetic defect of a mutant cell line deficient in UDP-galactose translocator. J Biochem 120:236–241.

Molinari F, Raas-Rothschild A, Rio M, Fiermonte G, Encha-Razavi F, Palmieri L, Palmieri F, Ben-Neriah Z, Kadhom N, Vekemans M, Attie-Bitach T, Munnich A, Rustin P, Colleaux L. 2005. Impaired mitochondrial glutamate transport in autosomal recessive neonatal myoclonic epilepsy. Am J Hum Genet 76:334–339.

Muntoni F. 2004. Journey into muscular dystrophies caused by abnormal glycosylation. Acta Myol 23:79–84.

Ng BG, Buckingham KJ, Raymond K, Kircher M, Turner EH, He M, Smith JD, Eroshkin A, Szybowska M, Losfeld ME, Chong JX, Kozenko M, et al. 2013. Mosaicism of the UDP-galactose transporter *SLC35A2* causes a congenital disorder of glycosylation. Am J Hum Genet 92:632–636.

Oelmann S, Stanley P, Gerardy-Schahn R. 2001. Point mutations identified in Lec8 Chinese hamster ovary glycosylation mutants that inactivate both the UDP-galactose and CMP-sialic acid transporters. J Biol Chem 276:26291–26300.

Okanishi T, Saito Y, Yuasa I, Miura M, Nagata I, Maegaki Y, Ohno K. 2008. Cutis laxa with frontoparietal cortical malformation: a novel type of congenital disorder of glycosylation. Eur J Paediatr Neurol 12:262–265.

Saitsu H, Kato M, Koide A, Goto T, Fujita T, Nishiyama K, Tsurusaki Y, Doi H, Miyake N, Hayasaka K, Matsumoto N. 2012a. Whole exome sequencing identifies *KCNQ2* mutations in Ohtahara syndrome. Ann Neurol 72:298–300.

Saitsu H, Kato M, Mizuguchi T, Hamada K, Osaka H, Tohyama J, Uruno K, Kumada S, Nishiyama K, Nishimura A, Okada A, Yoshimura Y, et al. 2008. *De novo* mutations in the gene encoding STXBP1 (MUNC18-1) cause early infantile epileptic encephalopathy. Nat Genet 40:782–788.

Saitsu H, Kato M, Okada I, Orii KE, Higuchi T, Hoshino H, Kubota M, Arai H, Tagawa T, Kimura S, Sudo A, Miyama S, et al. 2010. *STXBP1* mutations in early infantile epileptic encephalopathy with suppression-burst pattern. Epilepsia 51:2397–2405.

Saitsu H, Kato M, Osaka H, Moriyama N, Horita H, Nishiyama K, Yoneda Y, Kondo Y, Tsurusaki Y, Doi H, Miyake N, Hayasaka K, Matsumoto N. 2012b. *CASK* aberrations in male patients with Ohtahara syndrome and cerebellar hypoplasia. Epilepsia 53:1441–1449.

Saitsu H, Nishimura T, Muramatsu K, Kodera H, Kumada S, Sugai K, Kasai-Yoshida E, Sawaura N, Nishida H, Hoshino A, Ryujin F, Yoshioka S, et al. 2013. *De novo* mutations in the autophagy gene *WDR45* cause static encephalopathy of childhood with neurodegeneration in adulthood. Nat Genet 45:445–449.

Shen J, Gilmore EC, Marshall CA, Haddadin M, Reynolds JJ, Eyaid W, Bodell A, Barry B, Gleason D, Allen K, Ganesh VS, Chang BS, et al. 2010. Mutations in *PNKP* cause microcephaly, seizures and defects in DNA repair. Nat Genet 42:245–249.

Stromme P, Mangelsdorf ME, Shaw MA, Lower KM, Lewis SM, Bruyere H, Lutcherath V, Gedeon AK, Wallace RH, Scheffer IE, Turner G, Partington M, et al. 2002. Mutations in the human ortholog of Aristaless cause X-linked mental retardation and epilepsy. Nat Genet 30:441–445.

Wada Y, Azadi P, Costello CE, Dell A, Dwek RA, Geyer H, Geyer R, Kakehi K, Karlsson NG, Kato K, Kawasaki N, Khoo KH, et al. 2007. Comparison of the methods for profiling glycoprotein glycans–HUPO Human Disease Glycomics/Proteome Initiative multi-institutional study. Glycobiology 17:411–422.

Wada Y, Kadoya M, Okamoto N. 2012. Mass spectrometry of apolipoprotein C-III, a simple analytical method for mucin-type O-glycosylation and its application to an autosomal recessive cutis laxa type-2 (ARCL2) patient. Glycobiology 22:1140–1144.

Wang K, Li M, Hakonarson H. 2010. ANNOVAR: functional annotation of genetic variants from high-throughput sequencing data. Nucleic Acids Res 38:e164.

Weckhuysen S, Mandelstam S, Suls A, Audenaert D, Deconinck T, Claes LR, Deprez L, Smets K, Hristova D, Yordanova I, Jordanova A, Ceulemans B, et al. 2012. *KCNQ2* encephalopathy: emerging phenotype of a neonatal epileptic encephalopathy. Ann Neurol 71:15–25.

Wopereis S, Lefeber DJ, Morava E, Wevers RA. 2006. Mechanisms in protein O-glycan biosynthesis and clinical and molecular aspects of protein O-glycan biosynthesis defects: a review. Clin Chem 52:574–600.

Yoshioka S, Sun-Wada GH, Ishida N, Kawakita M. 1997. Expression of the human UDP-galactose transporter in the Golgi membranes of murine Had-1 cells that lack the endogenous transporter. J Biochem 122:691–695.

Hum Genet (2014) 133:225–234
DOI 10.1007/s00439-013-1372-6

ORIGINAL INVESTIGATION

A hemizygous *GYG2* mutation and Leigh syndrome: a possible link?

Eri Imagawa · Hitoshi Osaka · Akio Yamashita · Masaaki Shiina · Eihiko Takahashi · Hideo Sugie · Mitsuko Nakashima · Yoshinori Tsurusaki · Hirotomo Saitsu · Kazuhiro Ogata · Naomichi Matsumoto · Noriko Miyake

Received: 17 April 2013 / Accepted: 29 September 2013 / Published online: 8 October 2013

Abstract Leigh syndrome (LS) is an early-onset progressive neurodegenerative disorder characterized by unique, bilateral neuropathological findings in brainstem, basal ganglia, cerebellum and spinal cord. LS is genetically heterogeneous, with the majority of the causative genes affecting mitochondrial malfunction, and many cases still remain unsolved. Here, we report male sibs affected with LS showing ketonemia, but no marked elevation of lactate and pyruvate. To identify their genetic cause, we performed whole exome sequencing. Candidate variants were narrowed down based on autosomal recessive and X-linked recessive models. Only one hemizygous missense mutation (c.665G>C, p.W222S) in glycogenin-2 (*GYG2*) (isoform a: NM_001079855) in both affected sibs and a heterozygous change in their mother were identified, being consistent with the X-linked recessive trait. *GYG2* encodes glycogenin-2 (GYG2) protein, which plays an important role in the initiation of glycogen synthesis. Based on the structural modeling, the mutation can destabilize the structure and result in protein malfunctioning. Furthermore, in vitro experiments showed mutant GYG2 was unable to undergo the self-glucosylation, which is observed in wild-type GYG2. This is the first report of *GYG2* mutation in human, implying a possible link between GYG2 abnormality and LS.

Introduction

Glycogen is a large branched polysaccharide containing linear chains of glucose residues. Glycogen deposits in skeletal muscle and liver serve as shorter-term energy storage in mammals, while fat provides long-term storage. Glycogen biosynthesis begins with self-glucosylation of glycogenins by covalent binding of UDP-glucose to tyrosine residues of the glycogenins and the subsequent extension of approximately ten glucose residues (Pitcher et al. 1988; Smythe et al. 1988). Glycogen particles are formed by the continued addition of UDP-glucose to the growing

Electronic supplementary material The online version of this article (doi:10.1007/s00439-013-1372-6) contains supplementary material, which is available to authorized users.

E. Imagawa · M. Nakashima · Y. Tsurusaki · H. Saitsu · N. Matsumoto (✉) · N. Miyake (✉)
Department of Human Genetics, Yokohama City University Graduate School of Medicine, Yokohama 236-0004, Japan
e-mail: naomat@yokohama-cu.ac.jp

N. Miyake
e-mail: nmiyake@yokohama-cu.ac.jp

H. Osaka
Division of Neurology, Clinical Research Institute, Kanagawa Children's Medical Center, Yokohama 232-8555, Japan

A. Yamashita
Department of Molecular Biology, Yokohama City University School of Medicine, Yokohama 236-0004, Japan

M. Shiina · K. Ogata
Department of Biochemistry, Yokohama City University Graduate School of Medicine, Yokohama 236-0004, Japan

E. Takahashi
Division of Infection and Immunology, Clinical Research Institute, Kanagawa Children's Medical Center, Yokohama 232-8555, Japan

H. Sugie
Department of Pediatrics, Jichi Medical University, Tochigi 329-0498, Japan

glycogen chain by glycogen synthase, and introduction of branches every 10–14 residues by the glycogen branching enzyme (Krisman and Barengo 1975; Larner 1953). To date, two glycogenin paralogues have been identified in human, glycogenin-1 (GYG1) and glycogenin-2 (GYG2). These proteins have been shown to form homodimers, heterodimers and larger oligomers (Gibbons et al. 2002). GYG1 (muscle form) is expressed predominantly in muscle while GYG2 (liver form) is expressed mainly in liver, heart and pancreas (Barbetti et al. 1996; Mu et al. 1997). Biallelic GYG1 abnormality is known to cause muscle weakness and cardiac arrhythmia in humans through GYG1 autoglucosylation failure (Moslemi et al. 2010). However, human disease due to GYG2 abnormality has never been reported.

Leigh syndrome (LS; MIM #256000) was first described as a subacute necrotizing encephalomyelopathy by Dr. Denis Leigh in 1951 (Leigh 1951). LS is a progressive neurodegenerative disorder with an estimated incidence of 1:40,000 live births (Rahman et al. 1996). Onset is usually in early childhood (typically before age 2) (Naess et al. 2009; Ostergaard et al. 2007). Clinical manifestations of LS are observed in the central nervous system (CNS) (developmental delay, hypotonia, ataxia, convulsion, nystagmus, respiratory failure and dysphagia), peripheral nervous system (polyneuropathy and myopathy) and extraneural organs (deafness, diabetes, cardiomyopathy, kidney malfunction and others) (Finsterer 2008). The neurological features depend on the affected regions and degree of severity. The presence of bilateral, symmetrical, focal hyperintense T2-weighted MRI signals in basal ganglia (mainly putamen), thalamus, substantia nigra, substantia ruber, brainstem, cerebellum, cerebral white matter or spinal cord is diagnostic of LS (Farina et al. 2002; Medina et al. 1990). Neuropathological studies revealed that these lesions reflect neuronal necrosis, gliosis and vascular proliferation (Brown and Squier 1996; Leigh 1951). In the majority of LS cases, lactate, pyruvate or the lactate/pyruvate ratio is increased in blood and cerebrospinal fluid (Finsterer 2008). To the best of our knowledge, 37 nuclear genes are known to be mutated in LS, in addition to some mitochondrial genes (Antonicka et al. 2010; Debray et al. 2011; Finsterer 2008; Lopez et al. 2006; Martin et al. 2005; Quinonez et al. 2013). Thus, inheritance patterns of LS include mitochondrial, autosomal recessive and X-linked recessive modes (Benke et al. 1982; van Erven et al. 1987).

We encountered a Japanese family with affected brothers showing atypical LS without marked elevation of lactic or pyruvic acid and unknown etiology. A unique genetic variant was identified by whole exome sequencing (WES), which may be associated with atypical LS phenotype in this family.

Materials and methods

Subjects

Peripheral blood samples of affected brothers diagnosed with LS and their parents were collected after obtaining written informed consent. DNA was extracted from peripheral blood leukocytes using QuickGene-610L (Fujifilm, Tokyo, Japan) according to the manufacturer's instructions. Lymphoblastoid cell lines derived from all family members were established. The Institutional Review Boards of Yokohama City University School of Medicine approved this study.

Causative gene identification

Whole exome sequencing was performed in two affected individuals (II-2 and II-3 in Fig. 1a) as described in the Supplementary methods. All candidate variants based on autosomal and X-linked recessive models were checked by Sanger sequencing in the parents and affected siblings. PCR products amplified with genomic DNA as a template were sequenced on an ABI3500xl autosequencer (Applied Biosystems, Foster City, CA) and analyzed using Sequencher 5.0 (Gene Codes Corporation, Ann Arbor, MI). As the pedigree tree might also indicate mitochondrial inheritance of this disease and LS is known to be caused by mitochondrial genome mutations, we screened the entire mitochondrial genome by the algorithm reported previously (Picardi and Pesole 2012), using exome data (detailed in Supplementary methods).

Structure modeling

To evaluate the effect of the GYG2 missense mutation (c.665G>C, p.W222S in isoform a: NM_001079855) on its function at the molecular structural level, the mutated molecular structure was constructed, and the free energy change caused by the mutation was calculated using the FoldX software (version 3.0) (Guerois et al. 2002; Khan and Vihinen 2010). As crystal structure of human GYG2 is unavailable, that of human GYG1 (Protein Data Bank code; 3T7O) was used as a structural model. The mutation was introduced into one subunit of the GYG1 homodimer. The ligands included in the crystal structure of GYG1 were ignored in the calculation, because the FoldX energy function could not deal with the ligands. The calculation was repeated three times, and the resultant data were presented as an average value with standard deviations.

Preparation for mammalian expression vectors

Human glycogenin-2 isoform a cDNA clone (IMAGE Clone ID: 100008747) integrated in pENTR221 was purchased from Kazusa DNA Research Institute (Chiba, Japan). The